Masters Theses

Student Theses and Dissertations

2007

Artificial immune system based algorithms for optimization and self-tuning control in power systems

Mani Hunjan

Recommended Citation

ARTIFICIAL IMMUNE SYSTEM BASED ALGORITHMS FOR OPTIMIZATION

AND SELF-TUNING CONTROL IN POWER SYSTEMS

by

MANI HUNJAN

A THESIS

Presented to the Faculty of the Graduate School of the

UNIVERSITY OF MISSOURI-ROLLA

In Partial Fulfillment of the Requirements for the Degree

MASTER OF SCIENCE IN ELECTRICAL ENGINEERING

2007

Approved by

_____   _____
Ganesh Kumar Venayagamoorthy, Advisor   Keith A. Corzine

_____
Paula Lutz

PUBLICATION THESIS OPTION

This thesis consists of the following two articles that are intended for submission to the following publications:

Pages 1-41 are intended for submission to the IEEE TRANSACTIONS ON POWER SYSTEMS.

Pages 42-83 are intended for submission in IEEE TRANSACTIONS ON SYSTEM, MAN AND CYBERNETICS, PART C.

ABSTRACT

Artificial immune systems (AIS) are new computational intelligence methods inspired by various mechanisms of the biological immune system. AIS are adaptive systems inspired by theoretical immunology and its functions, principles and models. The work depicted in this thesis centers on the applications of AIS based algorithms for optimization and self-tuning control in power systems. The optimization is carried out using an algorithm based on the clonal selection principle and the self-tuning characteristics of control for parameters are inspired by the humoral immune response of the human body. The work in this thesis is written in two papers as follows:

Paper 1 - CSA is used to design multiple optimal power system stabilizers (PSS). The proper tuning of PSSs has a significant influence on its effectiveness in providing the required damping under different operating conditions and disturbances. CSA is used to determine the optimal parameters of four PSSs in a two area multi-machine power system. CSA optimized PSSs efficiently damp out the oscillations introduced in the system and its damping performance is slightly better than that of particle swarm optimization (PSO) optimized PSSs. The main contribution of CSA is that it converges faster and requires fewer computations than the standard PSO algorithm.

Paper 2 - CSA is used for optimization of four benchmark functions in literature. It is then used to design an optimal synchronous machine excitation controller which reduces oscillations introduced in the terminal voltage during disturbances. Immune feedback law is used to incorporate self-tuning characteristics in the optimal controller. The self-tuning optimal excitation controller reduces overshoot and settling time of oscillations. It also reduces power losses in the field circuit, thus, enhancing its life.

ACKNOWLEDGMENTS

I extend my sincere appreciation to all the people who made this thesis possible. First and foremost, I would like to thank my advisor Dr. Ganesh Kumar Venayagamoorthy, for his encouragement, guidance, co-operation and constant support throughout my graduate studies. He directed me in the right direction to tackle the problems I faced during my research.

In addition, I would also like to extend my gratitude to my thesis committee Dr. Keith A. Corzine and Dr. Paula Lutz for their insightful suggestions and comments which helped me shape my Masters research in a more realistic way.

I thank the Real-Time Power and Intelligent Systems (RTPIS) Laboratory for providing me with the right platform and environment to carry out my research.

I would also like to thank my family and my friend Tridib Das for their constant support and encouragement. Words cannot describe the extent of gratitude I owe to my mother, Sudha Hunjan, without whose selfless support and undying belief no work presented in this thesis would have begun. I will forever be grateful to my father, Virender Hunjan for always believing in me and inspiring me.

TABLE OF CONTENTS

LIST OF ILLUSTRATIONS

LIST OF TABLES

PAPER 1

A MODIFIED CLONAL SELECTION ALGORITHM FOR SIMULTANEOUS DESIGN OF MULTIPLE OPTIMAL POWER SYSTEM STABILIZERS

Mani Hunjan, *Student Member, IEEE* and

Ganesh K. Venayagamoorthy, *Senior Member, IEEE*

Abstract— **Power system stabilizers (PSSs) are added to enhance damping of power system oscillations in order to extend power transfer limits of the system and maintain reliable operation of the grid. They damp both inter-area and intra-area oscillations. The proper tuning of PSSs has a significant influence on its effectiveness in providing the required damping under different operating conditions and disturbances. This paper presents application of a modified clonal selection algorithm (CSA) to tune PSSs in the two-area four-machine benchmark power system. The modified CSA mutates the cells such that they are driven towards the antibody with the least fitness and hence, converges to the global optimum faster than the basic CSA. The optimal PSSs efficiently damp system oscillations during small and large disturbances. They exhibit good damping capabilities and oscillatory stability. The effectiveness and robustness of the CSA optimized PSSs is shown by comparing it with the particle swarm optimization (PSO) optimized PSSs and Conventional PSS for different disturbances and loading conditions.**

Index Terms – **Clonal selection algorithm, multi-machine power system, power system stabilizers.**

I. INTRODUCTION

Electrical power oscillations can occur on power systems that contain generators equipped with fast acting excitation systems. These oscillations occur when a large amount of power is transmitted over long transmission lines. Power oscillations of small magnitude and low frequency often persist for long periods of time. In some cases, this presents a limitation on the amount of power that can be transmitted within the system. Power System Stabilizers (PSSs) have been developed to aid in the damping of these power oscillations by modulating the excitation applied to the generator. They provide effective supplementary control by supplying auxiliary control signals to the excitation system of the generators.

In recent years, considerable effort has been placed on the design of multi-machine power system stabilizers. PSSs have been widely used to increase the damping ratios of electromechanical modes to suppress low frequency oscillations and increase oscillatory stability. These oscillations come into existence when rotors of generators oscillate with respect to each other using transmission line between them to exchange power. Depending on their location in the system, some generators participate in only one oscillation mode, while others participate in more than one mode. The conventional PSS used the lead-lag theory of phase compensation in the frequency domain and adjusted time of its correction signal (to change excitation) to oppose oscillations it detected in the generator rotor. It is tuned based on the linear model of the power system.

Recently, a number of approaches have been used to design and tune the parameters of the conventional PSS in order to obtain the optimal dynamic stability characteristics. These approaches are based on genetic algorithm [1-2], neural networks

[3-4], gradient descent methods [5], tabu search [6], simulated annealing [7], fuzzy logic [8], evolutionary programming [9], and particle swarm optimization [10]. These approaches however fail when dealing with epistatic objective functions (i.e. where parameters being optimized are highly correlated). Hence, an optimal PSS design is required which provides effective and rapid damping over a wide range of operating conditions.

An optimal PSS design using a modified clonal selection algorithm (CSA) is presented in this paper. The CSA is applied to determine the optimal parameters of the four PSSs in the two-area benchmark system. The response for the CSA optimized PSS is then compared with that obtained for the PSS optimized using particle swarm optimization (PSO).

This paper is organized as follows: Section II presents the two area multi-machine power system used in this study; Section III describes a modified CSA; Section IV describes the PSO algorithm; Section V describes the design of the optimal PSS; Section VI compares the performance of the CSA optimized and PSO optimized PSS; Section VII presents the simulation results obtained for the two area power system. Finally, conclusion and future work are given in Section VIII.

II. MULTI-MACHINE POWER SYSTEM

In spite of being a small test system, the two-area power system very closely mimics the behavior of typical systems in actual operation and is useful to study inter area oscillations, like those seen in large interconnected power systems [11]. The two area

power system shown in Fig. 1 consists of two fully symmetrical areas linked together by two transmission lines. Each area is equipped with two identical synchronous generators rated 20kV/900 MVA. All generators are equipped with identical speed governors and turbines, exciters and AVRs. All the four generators are also equipped with the PSS shown in Fig. 2. Load is represented as constant impedances and split between the areas in such a way that area 1 is exporting about 413 MW to area 2, under normal operating conditions [12].
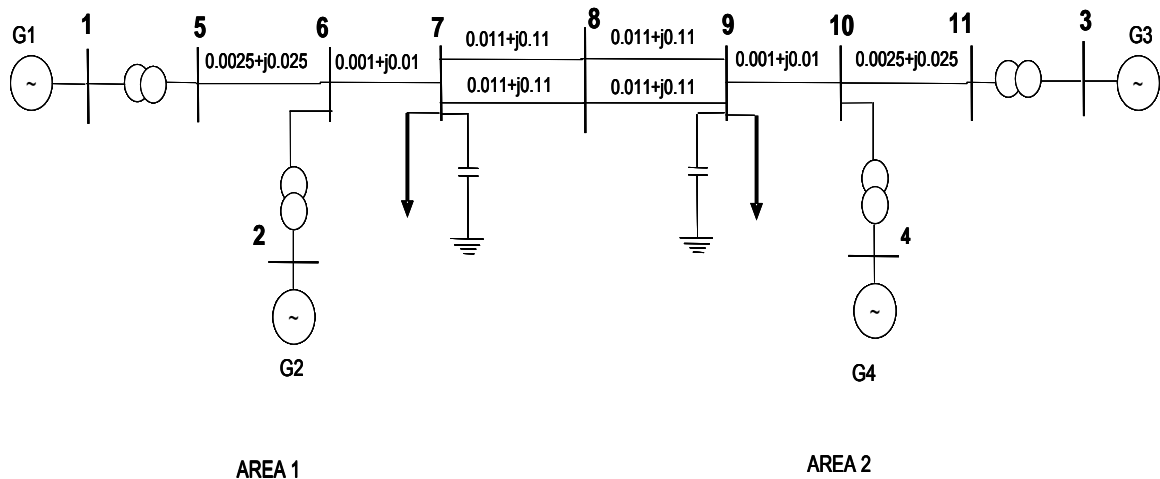
Fig. 1. Two area multi-machine power system.

Three electro-mechanical modes of oscillation are present in this system; two inter-plant (or intra-area) modes, one in each area, and one inter-area low frequency mode, in which the generating units in one area oscillate against those in the other area. Intra-area (0.8-2 Hz) oscillations are inherent in large interconnected power systems and they occur between two electrically close generation plants. Inter-area oscillations (0.2-0.8 Hz) are low frequency electromechanical oscillations. They are associated with groups of

generators in one geographical region swinging with respect to other groups in a different region interconnected through tie-lines. Adequate damping of these oscillations is a pre-requisite for secure operation of the system.

The PSSs detect the variation in the rotor speed ($\Delta\omega_{Gn}$), and provide an additional input signal (V_{pss}) to the excitation system of the generator to reduce the power swings in the system rapidly. A typical PSS block diagram is shown in Fig. 2. It consists of an amplifier block of gain constant K, a block having a washout time constant T_W and two lead lag compensators with time constants T_1 to T_4.
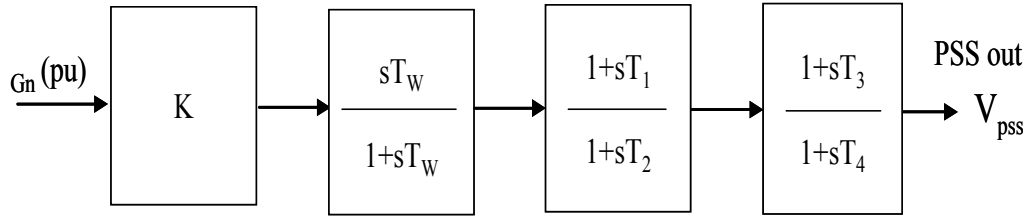
Fig. 2. Block diagram of a power system stabilizer.

III. CLONAL SELECTION ALORITHM

The clonal selection theory was introduced by F. M. Burnet in 1958 [13]. The clonal selection principle describes the response of the immune system to antigen [14]. Its principle is based on the fact that only certain T and B cells are selected for destruction of specific antigens invading the body. The selected T and B cells then proliferate to eliminate the antigen. The main features of the current clonal selection theory are that:

- Stimulation of certain T and B cells by antigens causes proliferation and differentiation.

- Non-stimulated cells are suppressed.

- The new cells generated are mutated clones of the parents (affinity maturation) representing a generation with random genetic changes. The mutation rate is proportional to the cell affinity.

- Newly differentiated lymphocytes which carry self reactive or low-affinity antigenic receptors are eliminated.

The core of the biological immune response is the clonal selection principle or the clonal selection theory. When B cells encounter antigens, they are activated to produce antibody molecules. B cells are lymphocytes and bear antigen receptors of a single specificity. Each B cell can produce only one kind of specific antibody molecules capable of recognizing and binding to this specific antigen. And it is this binding that stimulates the B cell to reproduce a cell or cells and later differentiate into plasma cells. This asexual proliferation generates daughter cells or clone cells. Therefore, only those cells that recognize the antigen proliferate, thus being selected against those that do not.

Clonal selection principle or algorithm has found applications in pattern recognition and optimization. The clonal selection algorithm basically consists of two populations; a set of antigens (*Ag*) and a set of antibodies (*Ab*). The basic CSA [15] is slightly modified by mutating the cloned population such that the new set of antibodies generated after maturation drive the algorithm towards the global optimum. The modified CSA used for optimization can be described as follows and its flowchart is depicted in Fig. 3.
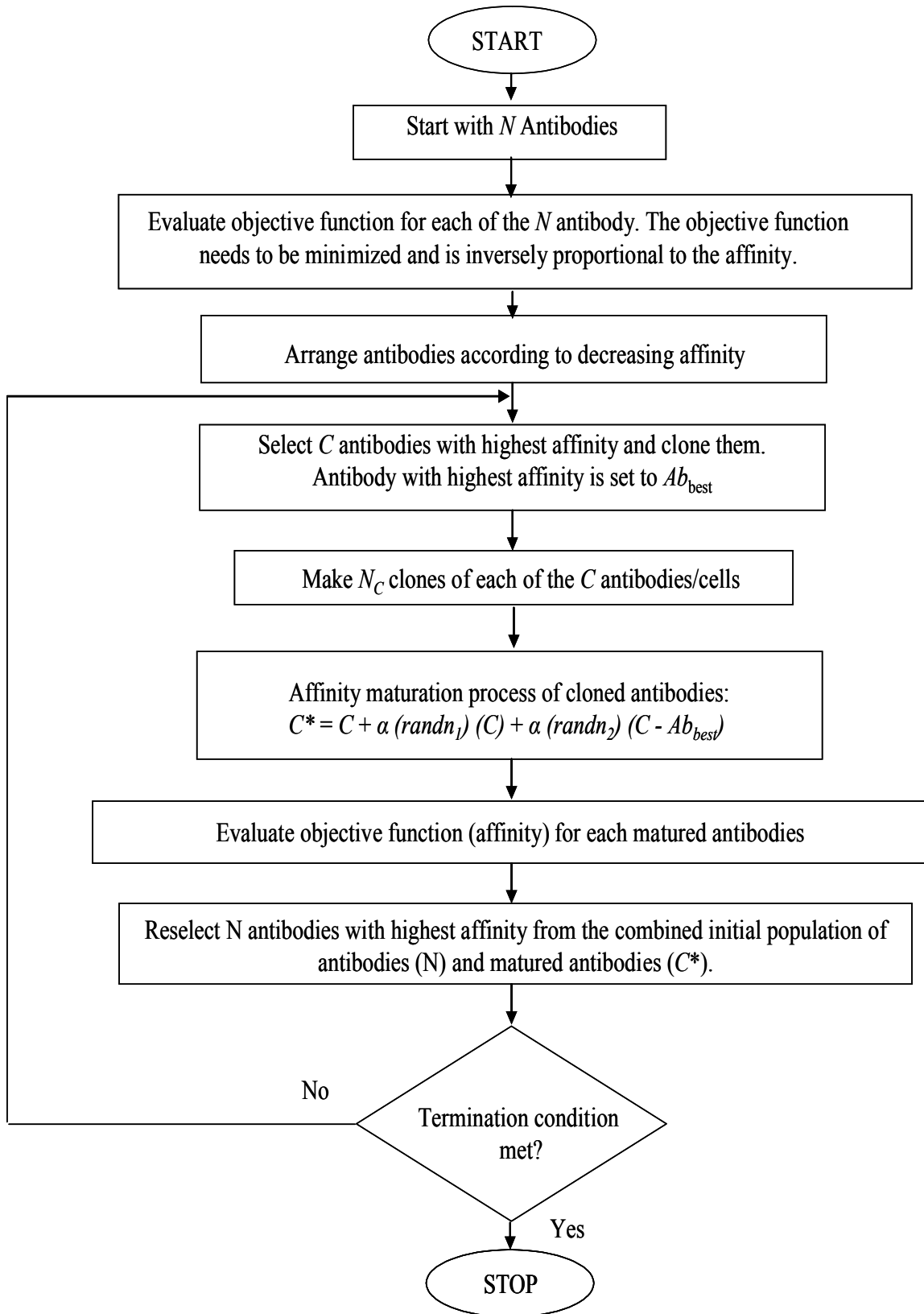
Fig. 3. Flowchart for the modified clonal selection algorithm.

1) Randomly generate a population of N antibodies.

2) Determine affinity of Ag to all the N antibodies. For optimization problems the affinity could be directly proportional or inversely proportional to the objective function that needs to be maximized or minimized.

3) Select C antibodies with highest affinity.

4) Clone the C selected antibodies (In the biological immune system B cells clone and produce antibodies). The number of clones generated for each of the antibodies can be given by

$$N_C = round\,(\beta.N) \tag{1}$$

where N_c is number of clones generated for each antibody, β is a multiplying factor, N is the total number of antibodies, and round ( ) is an operator which rounds its argument to the closest integer.

5) Store the antibody with the greatest affinity as Ab_{best}.

6) The cloned set of antibodies next undergoes affinity maturation. This affinity maturation is inversely proportional to the antigenic affinity. The higher the antigenic affinity, the lower the mutation rate. The affinity maturation of the cloned antibodies is calculated using

$$C^* = C + \alpha\,(rand_1)C + \alpha\,(rand_2)(C - Ab_{best}) \tag{2}$$

where C^* is the set of population obtained after cloning and affinity maturation of the C antibodies, α is calculated using

$$\alpha = \exp(-f) \tag{3}$$

where f is the normalized fitness or objective function of the antibody being mutated. $rand_1$ and $rand_2$ are random numbers in a uniform distribution between 0 and 1. The

affinity maturation of the cloned antibodies tends to drive the next set of antibodies towards the global optimum by taking into consideration the antibody with the greatest affinity (Ab_{best}).

7) Determine the antigenic affinity of the matured antibodies.

8) Reselect N antibodies with the highest affinity and repeat step 3 until some termination condition is satisfied.

The modified CSA summarized above has been used for optimization of PSS parameters for the two-area system.

IV. PARTICLE SWARM OPTIMIZATION

Particle swarm optimization (PSO) combines social psychology principles in socio-cognition human agents and evolutionary computations. The beauty of PSO lies in its ability to explore and exploit the search space by varying the parameters of the PSO according to its velocity and position update equations. This unique feature of the algorithm overcomes the premature convergence problem and enhances the search capability. Hence, it is a suitable optimization tool. PSO is a form of evolutionary computation technique (a search method based on natural systems) developed by Kennedy and Eberhart [16]-[18]. PSO like GA is a population (swarm) based optimization tool. However, unlike in GA, individuals are not eliminated from the population from one generation to the next. One major difference between particle swarm and traditional evolutionary computation methods is that particles' velocities are

adjusted, while evolutionary individuals' positions are acted upon; it is as if the "fate" is altered rather than the "state" of the particle swarm individuals [19].

The system initially has a population of random solutions. Each potential solution, called *particle*, is given a random velocity and is flown through the problem space. The particles have memory and each particle keeps track of previous best position and corresponding fitness. The previous best value is called the *pbest* of the particle and represented as p_{id}. Thus, p_{id} is related only to a particular particle i. The best value of all the particles' *pbest*s in the swarm is called the *gbest* and is represented as p_{gd}. The basic concept of PSO technique lies in accelerating each particle towards its p_{id} and the p_{gd} locations at each time step. The amount of acceleration with respect to both p_{id} and p_{gd} locations is given random weighting.

The following steps explain the procedure in the standard PSO algorithm.

1) Initialize a population of particles with random positions and velocities in d dimensions of the problem space.

2) For each particle, evaluate the desired optimization fitness function.

3) Compare every particle's fitness evaluation with its pbest value, p_{id}. If current value is better than p_{id}, then set p_{id} value equal to the current value and the p_{id} location equal to the current location in d-dimensional space.

4) Compare the updated pbest values with the population's previous gbest value, p_{gd}. If any of pbest values is better than p_{gd}, then update p_{gd} and its parameters.

5) Compute the new velocities and positions of the particles according to (4) and (5) respectively. v_{id} and x_{id} represent the velocity and position of ith particle in d^{th} dimension respectively and, *rand₁* and *rand₂* are two uniform random functions.

$$v_{id} = w \times v_{id} + c_1 \times rand_1 \times (p_{id} - x_{id})$$
$$+ c_2 \times rand_2 \times (p_{gd} - x_{id}) \tag{4}$$

$$x_{id} = v_{id} + x_{id} \tag{5}$$

6) Repeat from step 2 until a specified terminal condition is met, usually a sufficiently good fitness or a maximum number of iterations.

The PSO parameter in (4), w is called the inertia weight, which controls the exploration and exploitation of the search space. Local minima are avoided by small local neighborhood, but faster convergence is obtained by larger global neighborhood and in general, global neighborhood is preferred. c_1 and c_2 termed as cognition and social components respectively are the acceleration constants which changes the velocity of a particle towards p_{id} and p_{gd}.

V. OPTIMAL PSS DESIGN

The PSS has five parameters; one gain (K) and four lead-lag compensator time constants (T_1, T_2, T_3 and T_4). Proper tuning of a PSS has significant influence on its effectiveness in providing the required damping under different operating conditions. The optimal parameters for the four PSS in the two area system are obtained using CSA and PSO. The objective function is designed so as to minimize overshoot and settling time of system oscillations. An eigenvalue based objective function reflecting damping factor of each of the electromechanical eigenvalues at a number of different operating conditions is formulated. The optimization algorithm must minimize the cost function given by:

$$M = aM_1 + (1-a)M_2 \tag{6}$$

where

$$M_1 = \sum_{j=1}^{NP} \sum_{\sigma_{i,j} \geq \sigma_0} (\sigma_{i,j} - \sigma_0)^2 \tag{7}$$

$$M_2 = \sum_{j=1}^{NP} \sum_{\varsigma_{i,j} \leq \varsigma_0} (\varsigma_{i,j} - \varsigma_0)^2 \tag{8}$$

a is the weighing factor taken to be 0.1 for this study. NP is the number of operating points considered in the design. $\sigma_{i,j}$ is the real part of the ith eigenvalue under j^{th} operating condition considered. The value of σ_o determines the relative stability in terms of damping factor margin provided for constraining the placement of eigenvalues during the process of optimization. The closed loop eigenvalues are placed in the region to the left of the line as shown in Fig. 4 (a) if only M_1 is to be taken as the objective function. Similarly if M_2 is to be taken as the objective function then it limits the maximum overshoot of the eigenvalues as shown in Fig. 4 (b). In case of M_2, ζ_0 is the minimum damping factor to be achieved for all of the eigenvalues. When the cost function is as given by (6), it takes into account both damping and overshoot, and the eigenvalues are restricted within the D-shaped area as shown in Fig. 4 (c).

Limits are placed on the PSSs parameters to keep the system within the stability margin during optimization. The range of the parameters chosen in this study is selected keeping Kundur's settings [12] in mind. The maximum and the minimum values of these parameters are chosen such that the system does not lose its stability when the PSSs parameters attain any of these limits. The limits used are : $5 \leq K \leq 30, 0.01 \leq T_1 \leq 5.0,$ $0.01 \leq T_2 \leq 5.0, 0.1 \leq T_3 \leq 10, 0.1 \leq T_4 \leq 10.$
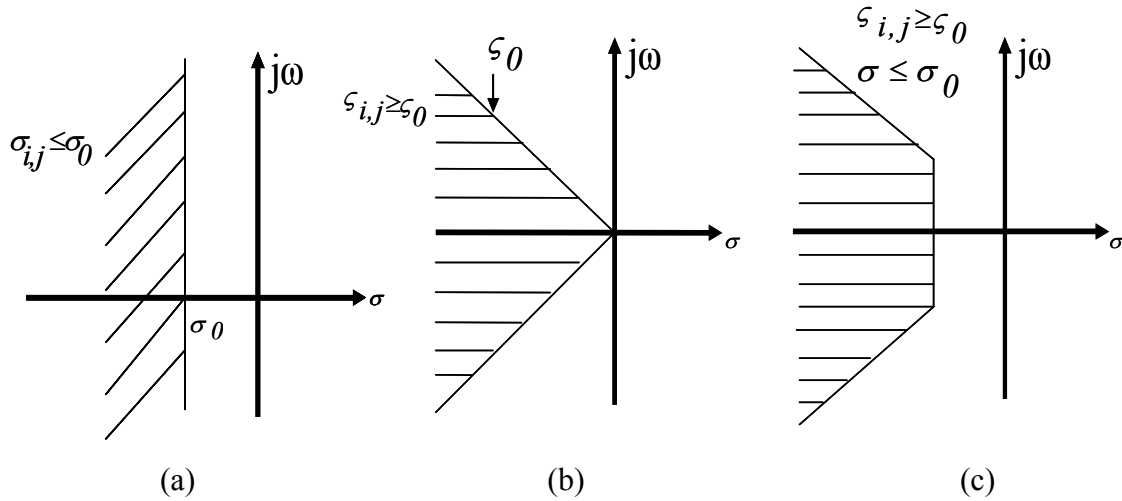
Fig. 4. Regions of location of eigenvalues for different objective functions.

VI. PERFORMANCE COMPARISON

The performance of the CSA and PSO optimized PSS is compared with Kundur's PSS [12] for the four operating conditions given in Table I.

Table I
Operating Conditions

Condition	Power Transfer (MW)	Load in Area 1 (MW)	Load in Area 2 (MW)
I	246	1120	1180
II	398	967	1767
III	446	920	1380
IV	476	890	1410

The following subsections compare the computational complexities of the CSA and PSO algorithms and the oscillatory modes obtained based on eigenvalue analysis,

and transient energy analysis of the damping response of the CSA and PSO algorithm optimized PSSs.

A. Computational Complexities

The number of fitness evaluations in PSO is *n* for a single iteration, where *n* is the number of particles. Similarly for CSA, the number of fitness evaluations is *m* for a single generation, where *m* is the number of antibodies. Table II provides us with the information of the computational complexity involved in CSA and PSO. The number of fitness evaluations in PSO is more than that of CSA. For 20 trials CSA on an average required lesser number of iterations to converge to zero than PSO. The average iterations PSO required to converge are 16.05 iterations whereas CSA required only 10.45 iterations to converge to zero. For the same number of particles employed, the fitness evaluation comparison can be seen in Table II. The number of additions and multiplications in comparison to PSO are both reduced by 47.82 %, respectively, while the number of fitness evaluations is reduced by 34.78 %.

Both of the algorithms are further compared in terms of their convergence speed with respect to the number of fitness evaluations. The average fitness of both CSA and PSO over the number of fitness evaluations are plotted as shown in Fig. 5. Average fitness of the particle in case of CSA takes lesser number of evaluations to converge to zero. Hence in a condition where computational complexity will be a priority, CSA will have an upper hand over PSO.

Table II

Comparison of Computational Complexity of PSO & CSA For PSS Design

(d = Number of dimensions)

Algorithms	Number of Fitness Evaluations	Number of Additions	Number of Multiplications
PSO – n particles (n=20, d=5)	$n \times$ number of iterations (460)	$5 \times n \times d \times$ number of iterations (115,000)	$5 \times n \times d \times$ number of iterations (115,000)
CSA – m antibodies (m=20, d=5)	$m \times$ number of iterations (300)	$4 \times m \times d \times$ number of iterations (6,000)	$4 \times m \times d \times$ number of iterations (6,000)
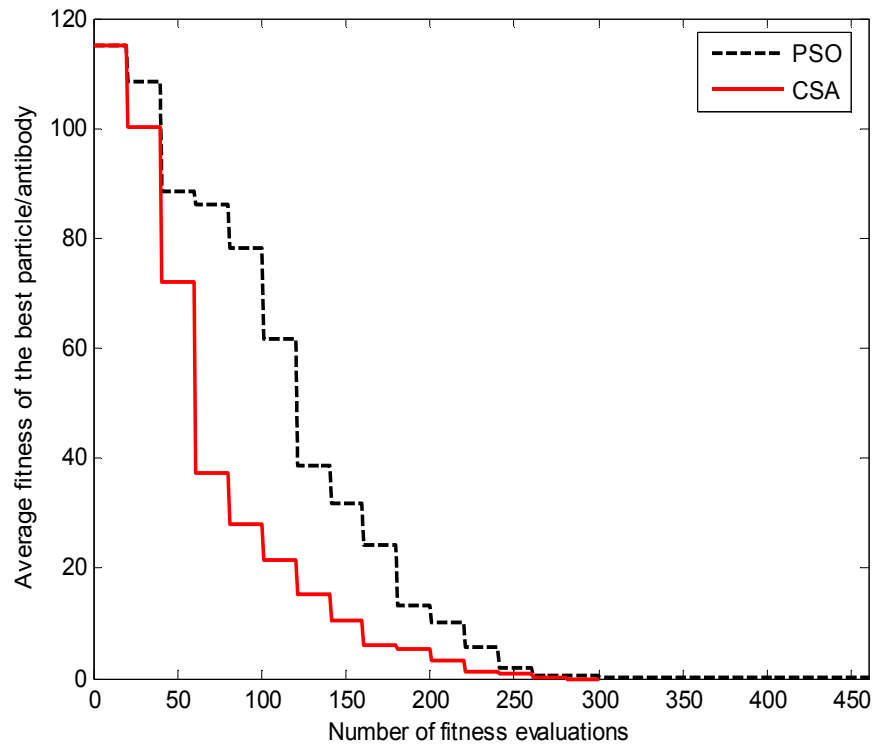
Fig. 5. Average fitness of the best particle/antibody over 20 trials.

B. Eigenvalue Analysis

Eigenvalue analysis is carried out on the system for different operating points. The system is optimized in such a fashion that the eigenvalues between the frequency range of 0.4-1.2 Hz must have damping greater than 0.4 and their real parts lie to the left of the -1.0 in the s-plane. The frequency range is chosen keeping in view the modal oscillations which lie in the low frequency range. The optimization techniques after certain number of iterations converges to zero indicating the no availability of the weakly damped modes in the system between the desired frequency range. This means that the eigenvalues lie in the D-shaped region as shown in Fig. 4. The electromechanical modes and the dampings are given in Tables III-VI for operating conditions I-IV. The optimal PSS parameters using CSA and PSO are determined over 20 trails. The best sets of optimal parameters for the PSS are given in Table A.1. in the Appendix. Tables III-VI also give the standard deviation and the minimum and maximum damping obtained for the different operating conditions.

It is seen that the system damping effect is enhanced and the dynamic characteristics are improved when using optimal PSSs. The location of the real parts of the electromechanical modes of interest for the CSA optimized PSSs are more towards the left of the -1.0 line than the PSO optimized PSSs or Kundur's PSS [12]. The CSA optimized PSSs are the best damping providers for all the four operating conditions. The novelty of the optimization techniques can be further seen as the local modes of oscillations of the generators are absent in the system with the PSO and CSA optimized PSSs.

Table III

Oscillatory Modes of the System- Operating Condition I

Parameters	Eigenvalue	Freq (Hz)	Damping (%)	Dominant States
Kundur	-0.96 ± j 4.22	0.67	22.2	Inter Area Mode
	-6.28 ± j 7.08	1.12	66.3	Local Mode
	-5.64 ± j 7.26	1.15	61.3	Local Mode
PSO	-1.73 ± j 3.66	0.58	41.67 ± 0.7163 (40.75, 42.75)	Inter Area Mode
CSA	-1.75± j 3.62	0.57	42.31 ± 1.1031 (40.72, 43.89)	Inter Area Mode

Table IV

Oscillatory Modes of the System- Operating Condition II

Parameters	Eigenvalue	Freq (Hz)	Damping (%)	Dominant States
Kundur	-0.95 ± j 4.05	0.64	22.9	Inter Area Mode
	-6.27 ± j 7.12	1.13	66.8	Local Mode
	-5.43 ± j 7.38	1.17	59.2	Local Mode
PSO	-1.72 ± j 3.53	0.56	42.76 ± 0.7352 (41.83, 43.87)	Inter Area Mode
CSA	-1.74 ± j 3.48	0.55	43.31 ± 0.9212 (41.94, 44.73)	Inter Area Mode

Table V

Oscillatory Modes of the System- Operating Condition III

Parameters	Eigenvalue	Freq (Hz)	Damping (%)	Dominant States
Kundur	-0.92 ± j 4.14	0.65	21.6	Inter Area Mode
	-6.26 ± j 7.13	1.13	65.9	Local Mode
	-5.62 ± j 7.26	1.15	61.2	Local Mode
PSO	-1.67 ± j 3.62	0.57	40.98 ± 0.7195 (40.00, 42.05)	Inter Area Mode
CSA	-1.70 ± j 3.57	0.57	41.60 ± 1.0553 (40.00, 43.13)	Inter Area Mode

Table VI

Oscillatory Modes of the System- Operating Condition IV

Parameters	Eigenvalue	Freq (Hz)	Damping (%)	Dominant States
Kundur	-0.91 ± j 4.12	0.65	21.5	Inter Area Mode
	-6.25 ± j 7.14	1.13	65.8	Local Mode
	-5.61 ± j 7.26	1.15	61.1	Local Mode
PSO	-1.66 ± j 3.61	0.57	40.90 ± 0.7161 (40.00, 41.97)	Inter Area Mode
CSA	-1.69 ± j 3.56	0.56	41.55 ± 1.0473 (40.00, 43.15)	Inter Area Mode

C. Transient Energy Analysis of Damping Response

This section compares the optimized PSSs with Kundur's PSSs [12] based on a performance index. Transient energy is the energy existing in the oscillations of the generators rotor after a disturbance. The transient energy of each of the generator for the first 3 seconds after the fault has been calculated using equation (8)

$$TE_{Gen_i} = \frac{1}{2} H_{Gen_i} \int_{t_{flt}}^{t_{flt}+3} \Delta \omega_i^2 \, dt \qquad (9)$$

where *i* is the generator number, H_{Gen} is the inertia constant of the generator, and t_{flt} is the time the fault is triggered. The performance index (P.I.), given in (10), is a measure of how the system has performed under the given conditions with the different set of PSS parameters. The higher the performance indices the better the controller damping performance.

$$Performance\ Index\ (P.I.) = 1/\,TE \qquad (10)$$

Tables VII-X presents the normalized performance indices of Area 1 and Area 2 for the system subjected to two disturbances for four operating scenario mentioned in Table I. Table XI gives the overall normalized performance index for the four operating conditions. The tables show the normalized P.I.s of the areas. Normalized P.I.s are obtained by dividing the P.I.s by the P.I. of Kundur's in that row. Tables VII-XI show that the P.I. of the CSA optimized PSSs are the best in each row. The robustness of the optimization technique can be ascertained by observing the P.I.s in cases of a line outage, short circuit and overall performance. System having CSA optimized PSSs provide better damping to the oscillations as the P.I.s in those cases are improved in comparison to a system having Kundur's PSSs or PSO optimized PSS in all operating conditions.

Table VII

Normalized Performance Index for Operating Condition I

Disturbances	Areas	Kundur	PSO	CSA
Short Circuit	Area 1	1.0	1.7196	1.8358
	Area 2	1.0	2.3201	2.3752
Line Outage	Area 1	1.0	1.541	1.5822
	Area 2	1.0	1.4643	1.5061
Overall Performance	Area 1	1.0	1.6303	1.718
	Area 2	1.0	1.8992	1.9406

Table VIII

Normalized Performance Index for Operating Condition II

Disturbances	Areas	Kundur	PSO	CSA
Short Circuit	Area 1	1.0	2.0699	2.1417
	Area 2	1.0	1.9892	2.0068
Line Outage	Area 1	1.0	1.3693	1.4076
	Area 2	1.0	1.3798	1.4238
Overall Performance	Area 1	1.0	1.7196	1.7746
	Area 2	1.0	1.6845	1.7153

Table IX

Normalized Performance Index for Operating Condition III

Disturbances	Areas	Kundur	PSO	CSA
Short Circuit	Area 1	1.0	1.9747	2.0959
	Area 2	1.0	2.1668	2.1958
Line Outage	Area 1	1.0	1.3764	1.416
	Area 2	1.0	1.3821	1.4255
Overall Performance	Area 1	1.0	1.6755	1.7559
	Area 2	1.0	1.7744	1.8106

Table X

Normalized Performance Index for Operating Condition IV

Disturbances	Areas	Kundur	PSO	CSA
Short Circuit	Area 1	1.0	2.0292	2.1376
	Area 2	1.0	2.1294	2.1514
Line Outage	Area 1	1.0	1.3808	1.4202
	Area 2	1.0	1.3755	1.4186
Overall Performance	Area 1	1.0	1.705	1.7789
	Area 2	1.0	1.7524	1.7850

Table XI

Overall Normalized Performance Index

Operating Condition	Areas	Kundur	PSO	CSA
I	Area 1	1.0	1.6303	1.718
	Area 2	1.0	1.8992	1.9406
II	Area 1	1.0	1.7196	1.7746
	Area 2	1.0	1.6845	1.7153
III	Area 1	1.0	1.6755	1.7559
	Area 2	1.0	1.7744	1.8106
IV	Area 1	1.0	1.705	1.7789
	Area 2	1.0	1.7524	1.7850
Overall Performance	Area 1	1.0	1.6826	1.7568
	Area 2	1.0	1.7601	1.8128

VII. SIMULATION RESULTS

The effectiveness of the CSA and PSO optimized PSS is evaluated for the two-area multi-machine power system. The PSSs are tuned using CSA and PSO from the

frequency domain information. The objective function used for the optimization of PSS parameters is given by (6). The optimization is carried out by simultaneously taking into consideration the four operating conditions given in Table I. The optimal values are determined over 20 trials. Two tests are carried out for each of the operating conditions given in Table I: a 150 ms short circuit at bus 8, and permanent line outage between buses 7 and 8. The response of the generator speed, PSS output and tie line power transfer are shown for CSA and compared with PSO optimized and Kundur's PSS parameters [12]. The optimal PSS parameters using CSA and PSO are determined over 20 trials and the best set of optimal PSS parameters obtained are given in Table A.1 in the Appendix.

A. Test 1

A three phase short circuit of duration 150 ms is applied at bus 8 of the two area system given in Fig. 1. The short circuit is in the middle of the tie lines connecting the two areas of the system.

1) Operating Condition I :

The rotor speed responses of two generators in the system (one in each area), G1 and G3 are shown in Fig. 6. Similar responses were observed for generators G2 and G4. It is seen that the responses of PSO optimized PSS and CSA optimized PSS are better than that obtained using Kundur's parameters. The CSA optimized PSS damps out the oscillations effectively and attains the steady state value faster than Kundur's PSS and comparable to PSO optimized PSS.

The corresponding PSS output for PSS1 and PSS3 are shown in Fig. 7. The PSS outputs indicate that PSO and CSA optimized PSSs provide better control by better modulation of the excitation supplied to the generator. The power exported from area 1 to area 2 in Fig.1 is 246 MW. When there is any fault in the system this power transfer across the tie line is affected. Fig. 8 shows the oscillations in the tie line power (between area 1 and area 2) for a 150 ms short circuit at bus 8 for operating condition I. It can be seen that the oscillations are less for the CSA and PSO optimized PSS. This means that a steady power transfer between the two areas is restored faster for CSA optimized PSS as compared to Kundur's PSS. The performance of CSA and PSO optimized PSS is comparable.

Fig. 6. Speed response of generators G1 and G3 for a 150 ms three phase short circuit at bus 8 for operating condition I.

Fig. 7. Corresponding PSS outputs for PSS1 and PSS3 for a 150 ms three phase short circuit at bus 8 for operating condition I.

Fig. 8. Corresponding tie line power flow for 150 ms three phase short circuit at bus 8 for operating condition I.

2) Operating Condition II:

The generator speed response (for generators G2 and G4), corresponding PSSs output (PSS2 and PSS4) and tie line power flow for operating condition II are given in Figs. 9 to 11, respectively. From Fig. 9, it is seen that the CSA and PSO optimized PSSs exhibit the better response in terms of damping the oscillations introduced in the speed response of the generators of the system as compared to Kundur's PSS. The CSA and PSO optimized PSS parameters are shown to minimize the overshoot and damp the oscillations quickly and efficiently. The PSS outputs in Fig. 10 show that the optimal PSSs provide better modulation of the generator in comparison to Kundur's PSS. Fig.11 shows that the power transfer between the two areas is restored faster for CSA and PSO optimized PSS as compared to Kundur's PSS.
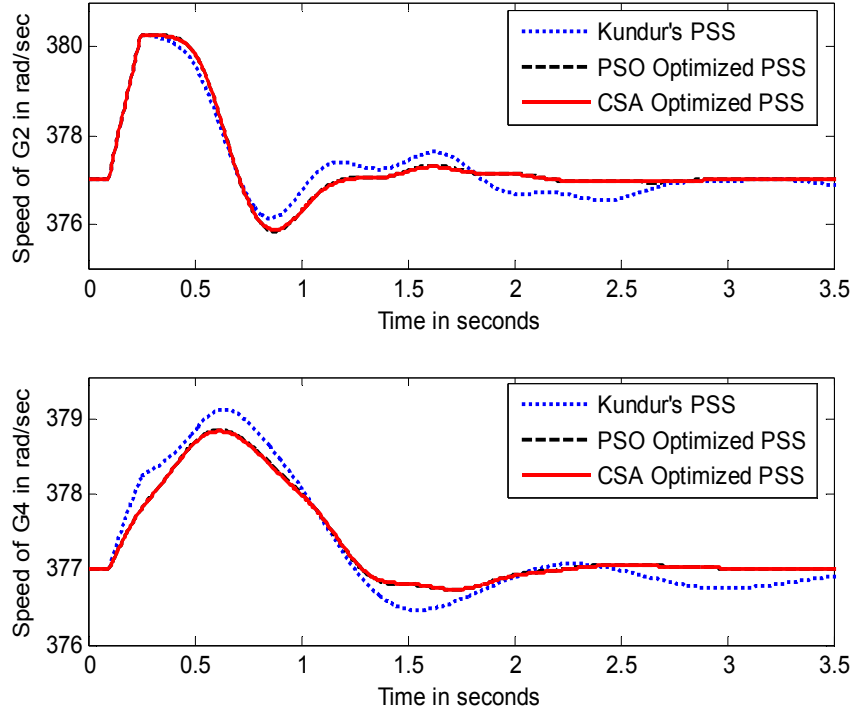
Fig. 9. Speed response of generators G2 and G4 for a 150 ms three phase short circuit at bus 8 for operating condition II.
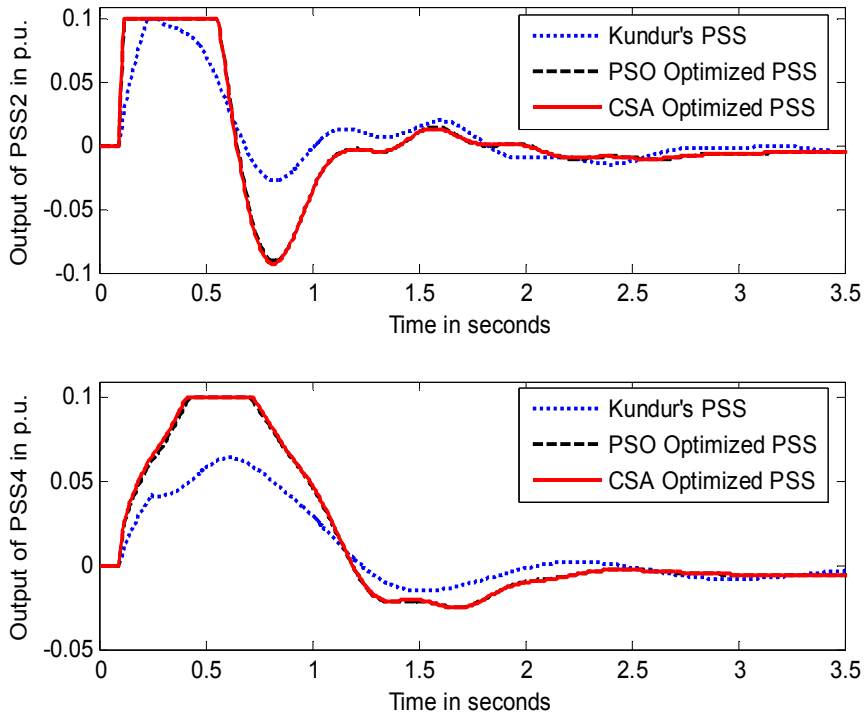
Fig. 10. Corresponding PSS outputs for PSS2 and PSS4 for a 150 ms three phase short circuit at bus 8 for operating condition II.
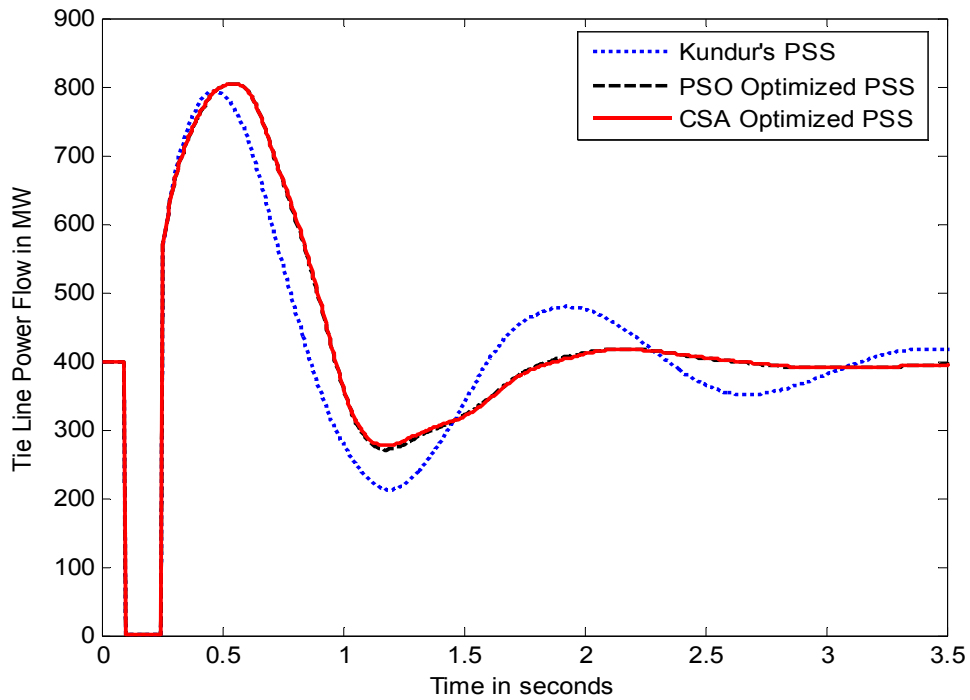
Fig. 11. Corresponding tie line power flow for 150 ms three phase short circuit at bus 8 for operating condition II.

3) Operating Condition III:

Various responses are observed for PSSs with optimized parameters for operating condition III. The generator speed responses, corresponding PSS output and the tie-line power flow are shown in Figs. 12 to 14 respectively.

It is seen that CSA and PSO optimized PSSs damp out the oscillations in the generator speed efficiently. The generator rotor speed settles to its steady state value much faster than with Kundur's PSS. The PSS outputs show that PSSs with CSA and PSO optimized parameters provide better auxiliary signals to the excitation system of the generator to damp the oscillations introduced due to the short circuit. Fig. 14 gives the tie line power flow oscillations after the short circuit. It is seen that the optimal PSSs bring about faster damping of power oscillations in the tie line as compared to Kundur's PSS.
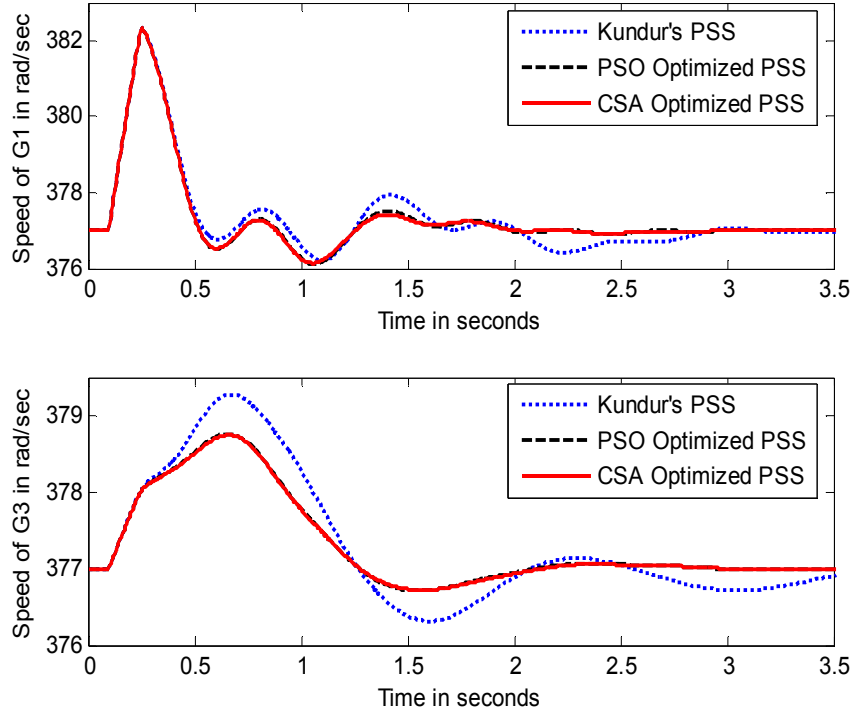
Fig. 12. Speed response of generators G1 and G3 for a 150 ms three phase short circuit at bus 8 for operating condition III.
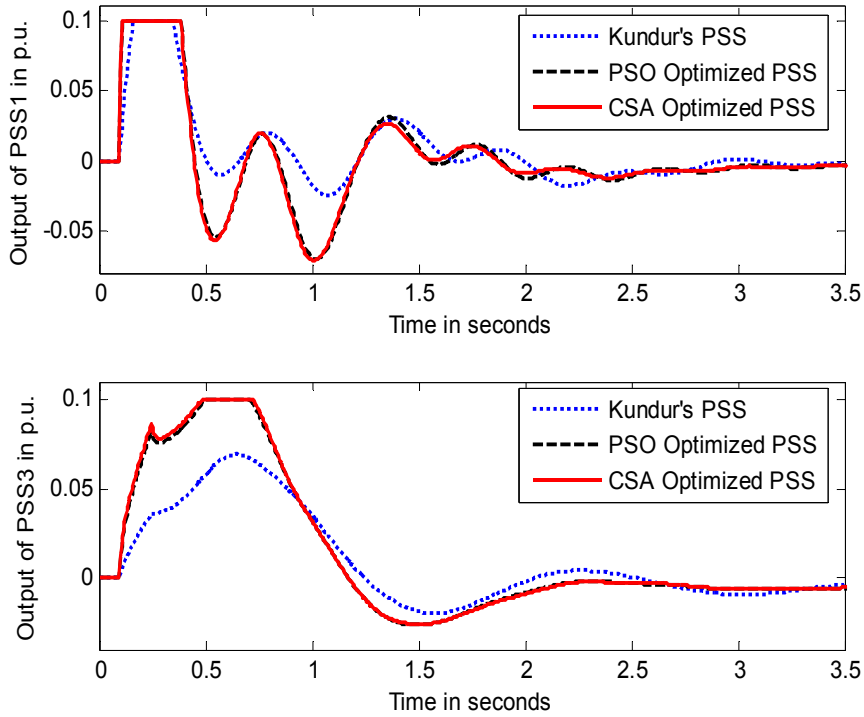
Fig. 13. Corresponding PSS outputs for PSS1 and PSS3 for a 150 ms three phase short circuit at bus 8 for operating condition III.
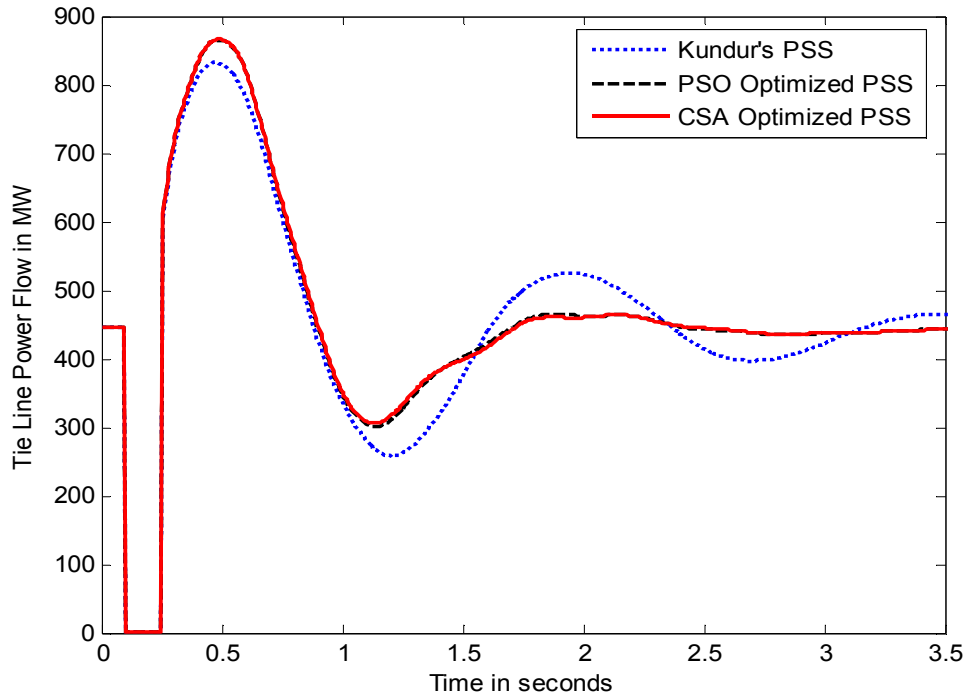
Fig. 14. Corresponding tie line power flow for 150 ms three phase short circuit at bus 8 for operating condition III.

4) Operating Condition IV:

Various responses are observed for PSSs with optimized parameters for operating condition IV. The generator speed responses, corresponding PSS output and the tie-line power flow are shown in Figs. 15 to 17, respectively.

As can be seen in Fig. 15, CSA and PSO optimized PSS damp the oscillations in the generator speed efficiently. The settling time of the generator speed response is significantly reduced for the optimal PSSs. The PSSs output in Fig. 16 show that the CSA and PSO optimized PSS make considerable effort to provide modulation of excitation supplied to the generators. The tie line power transfer in Fig. 17 shows that the oscillations in tie line power are greatly reduced for optimized PSS parameters as compared to the Kundur's PSS parameters.
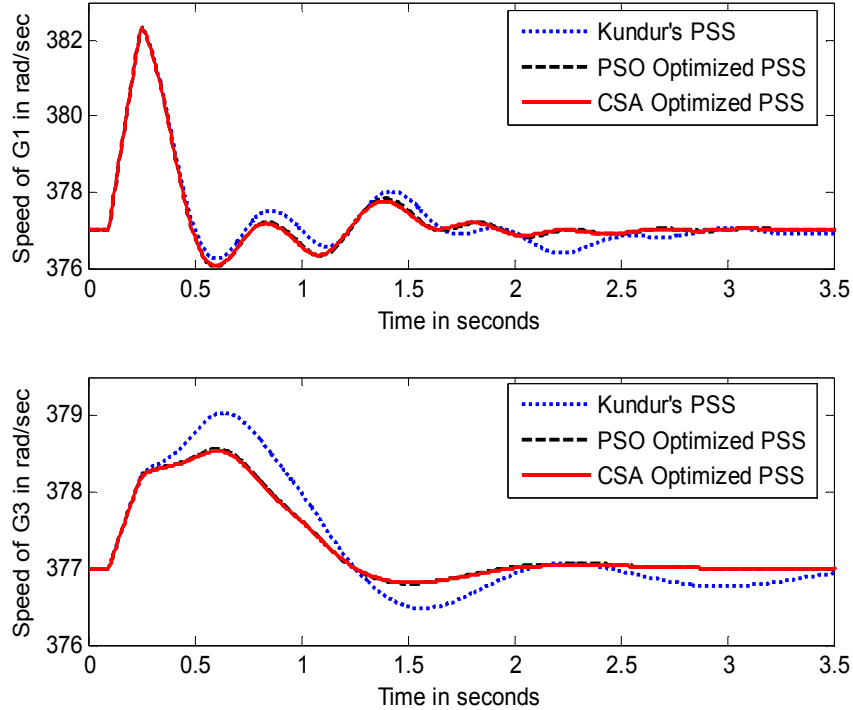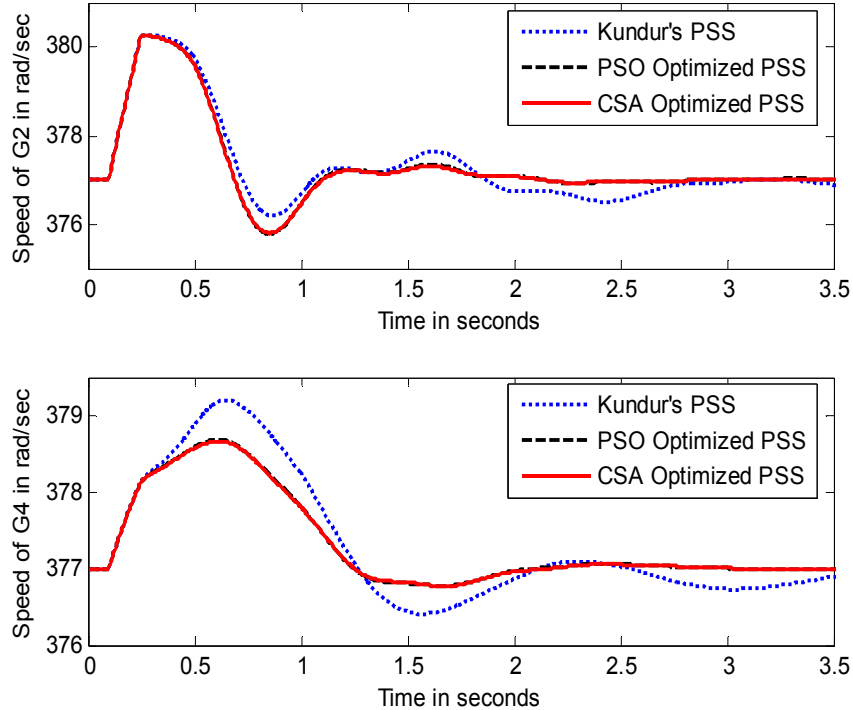
Fig. 15. Speed response of generators G2 and G4 for a 150 ms three phase short circuit at bus 8 for operating condition IV.
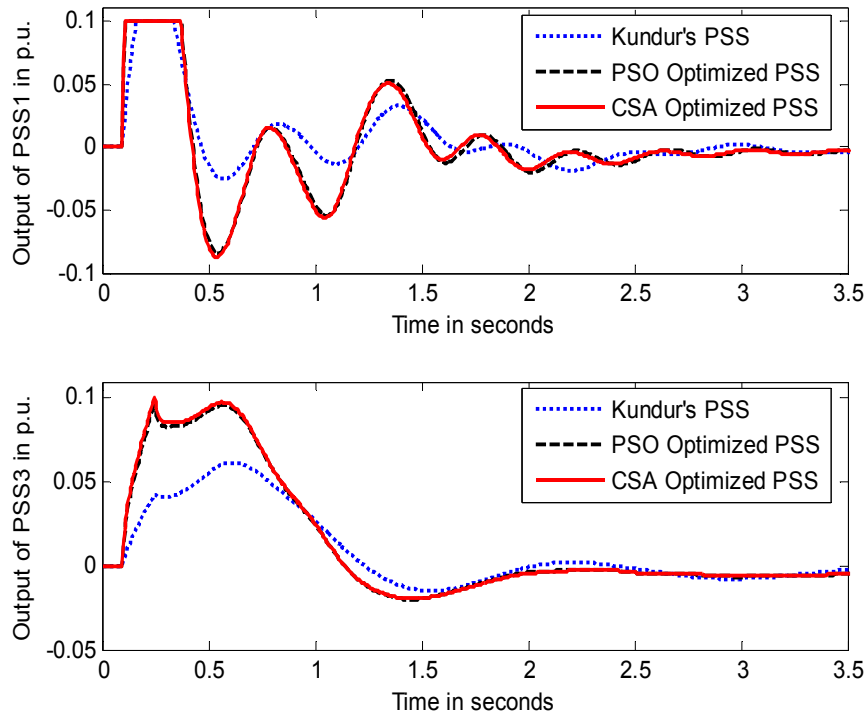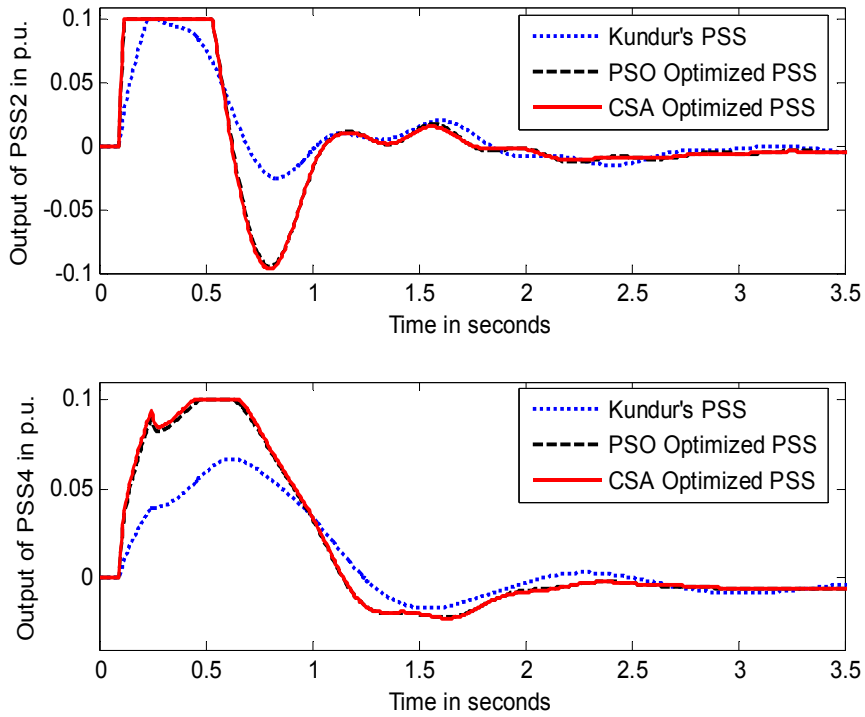
Fig. 16. Corresponding PSS outputs for PSS2 and PSS4 for a 150 ms three phase short circuit at bus 8 for operating condition IV.
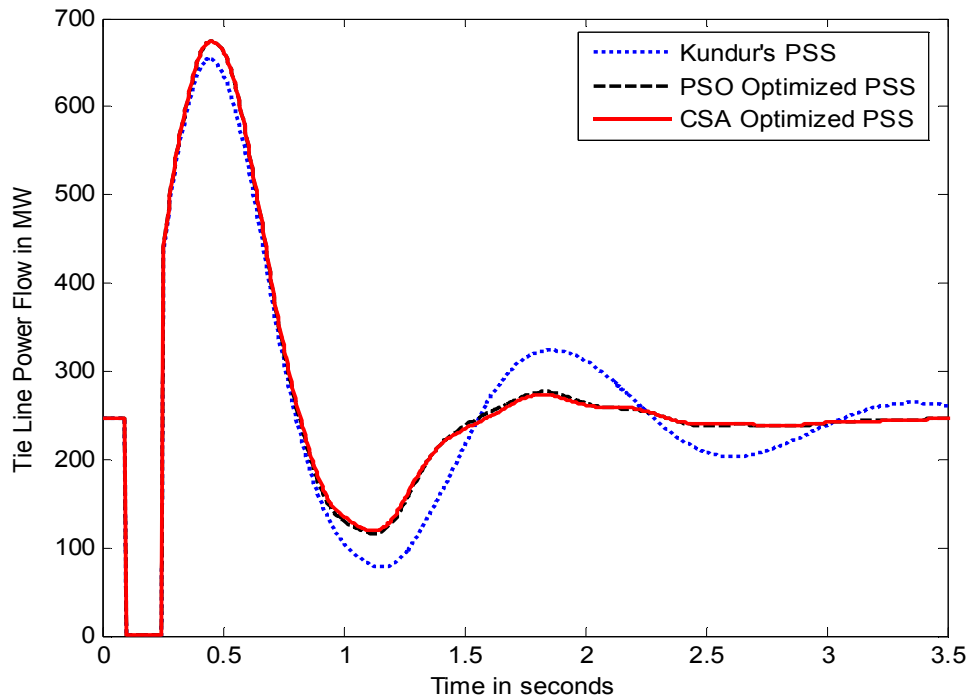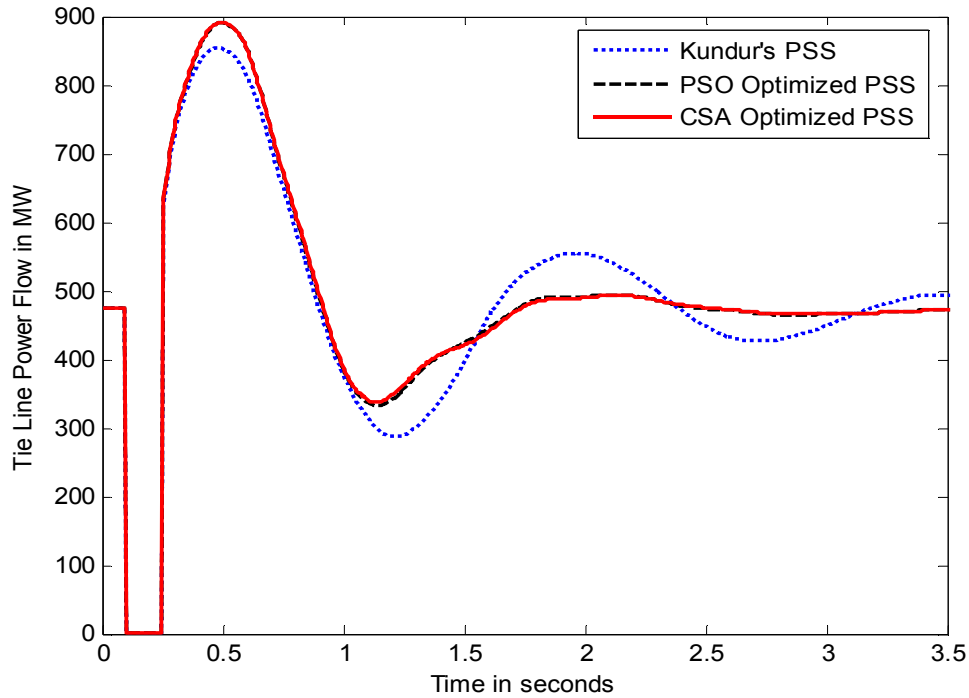

Fig. 17. Corresponding tie line power flow for 150 ms three phase short circuit at bus 8 for operating condition IV.

B. Test 2

A permanent line outage is applied between buses 7 and 8 of the two area system given in Fig. 1. Various responses are studied for the four operating conditions given in Table I for the permanent line outage.

1) Operating Condition I:

The speed of the generators (one in each area), the corresponding PSS outputs and the tie line power flow for operating condition I for a permanent line outage is given in Figs. 18 to 20, respectively.
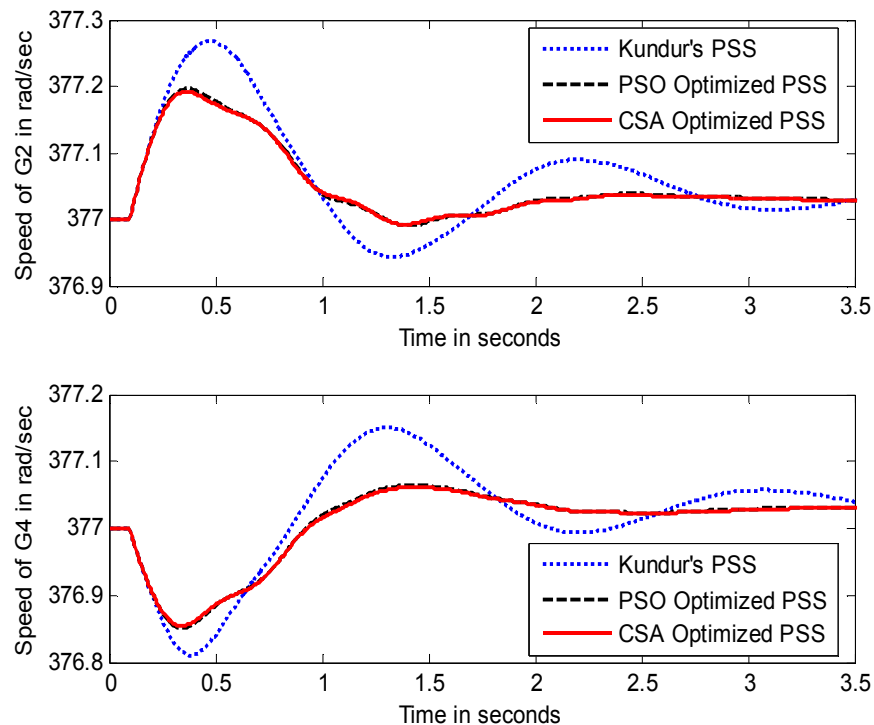
Fig. 18. Speed response of generators G2 and G4 for a permanent line outage between buses 7 and 8 for operating condition I.
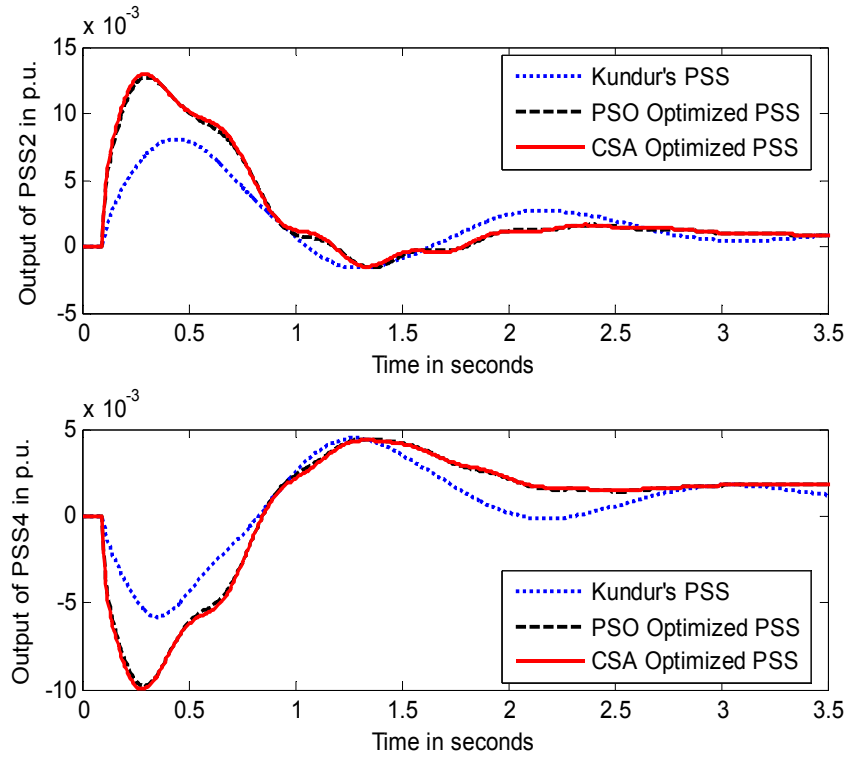
Fig. 19. Corresponding PSS outputs for PSS2 and PSS4 for a permanent line outage between buses 7 and 8 for operating condition I.
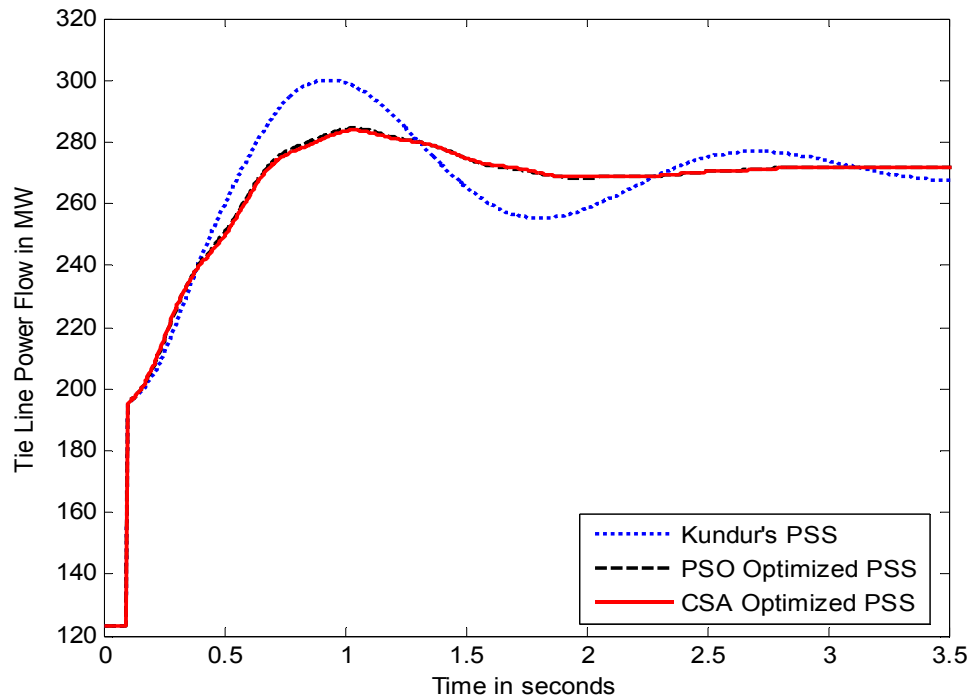
Fig. 20. Corresponding tie line power flow for a permanent line outage between buses 7 and 8 for operating condition I.

The speed response of the generators show that the oscillations are minimized by the CSA and PSO optimized PSSs. The overshoot and settling time of the deviations in the generator speed are minimized. It is also seen that the power transfer in the tie line is restored faster when using CSA and PSO optimized PSS as compared to the Kundur's PSS. The oscillations in tie line power are reduced and the overshoot is minimized significantly. The power flow through the tie line after the permanent line outage is restored faster for optimal PSSs.

2) Operating Condition II:

Various responses for the different PSSs are studies for operating condition II for a permanent line outage. The generator speed responses, corresponding PSS output and the tie-line power flow are shown in Figs. 21 to 23, respectively.

Fig. 21 gives the speed response of generator G1 and G3 (one in each area). Similar responses are observed for generators G2 and G4. It is seen that the generator speed oscillations settle down faster for CSA and PSO optimized PSS as compared to Kundur's PSS. The other two generators G2 and G4 also exhibit similar responses. The corresponding output of the PSSs is given in Fig. 22. It is seen that optimal PSSs exert an extra effort to provide appropriate modulation of excitation supplied to the generators. The tie line power flow shown in Fig. 23 indicates that the tie line power flow after the permanent line outage is restored to the required 446 MW faster for the optimal PSSs as compared to the Kundur's PSS. There are minimal oscillations in the tie line power for the optimal PSSs, while for Kundur's PSS the overshoot is high and the settling time is large.
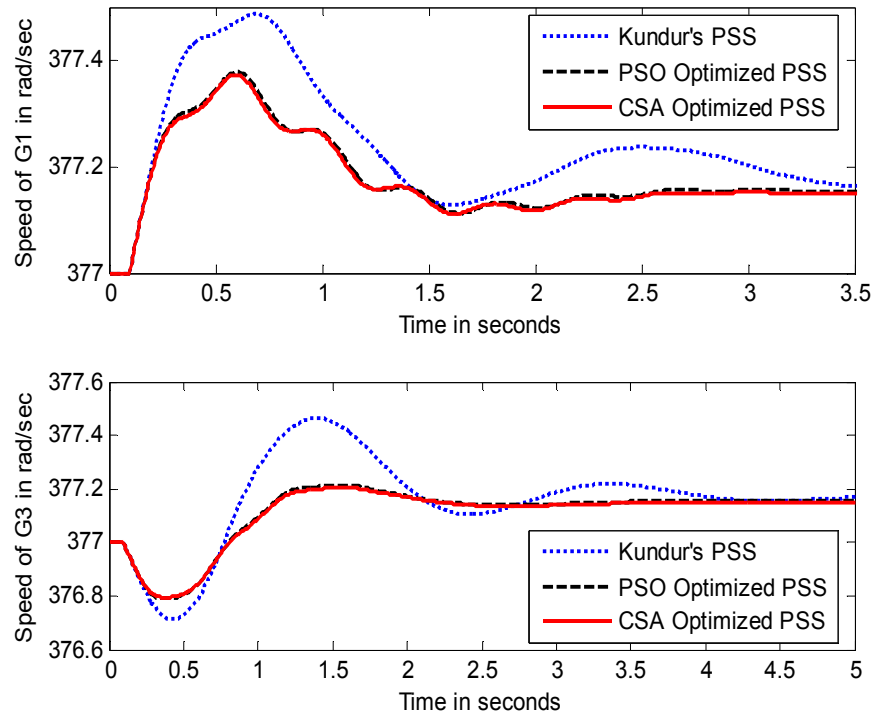
Fig. 21. Speed response of generators G1 and G3 for a permanent line outage between buses 7 and 8 for operating condition II.
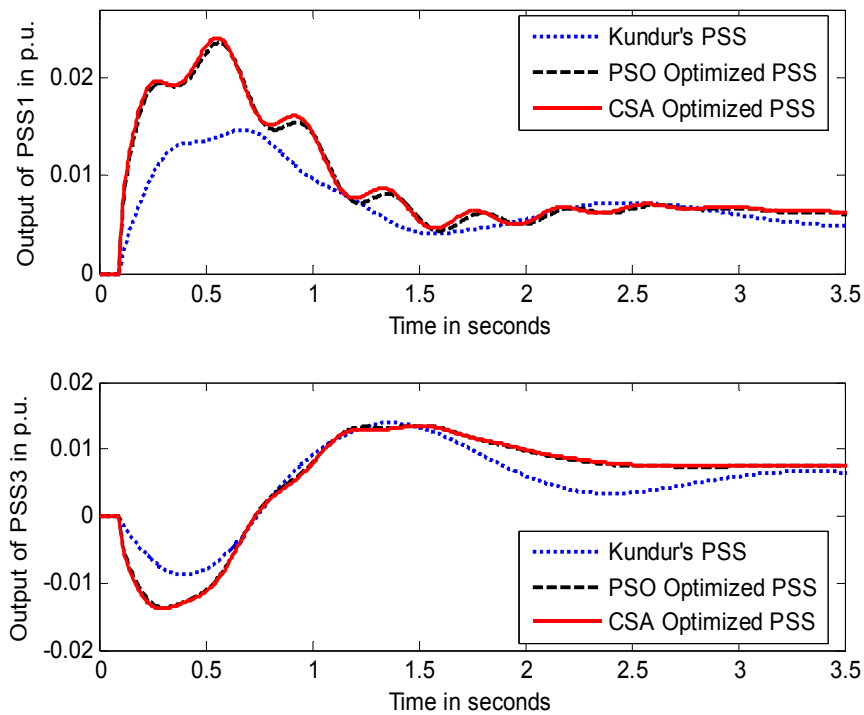
Fig. 22. Corresponding PSS outputs for PSS1 and PSS3 for a permanent line outage between buses 7 and 8 for operating condition II.
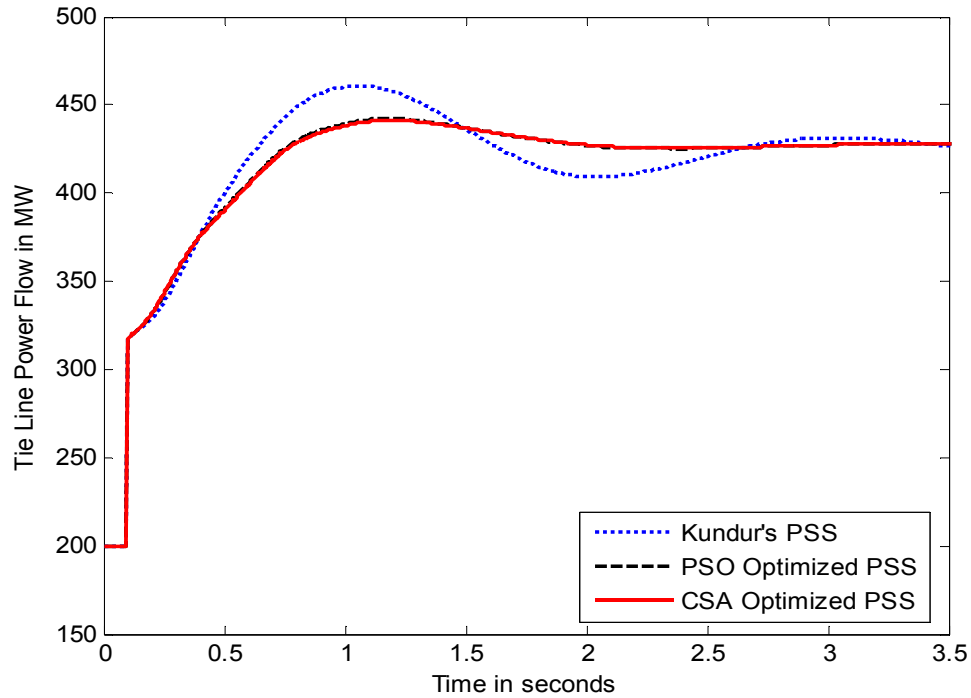
Fig. 23. Corresponding tie line power flow for a permanent line outage between buses 7 and 8 for operating condition II.

3) Operating Condition III:

Various responses are observed for PSSs with optimized parameters for operating condition III. The generator speed responses, corresponding PSS output and the tie-line power flow are shown in Figs. 24 to 26, respectively.

The speed responses clearly depict the superiority of the CSA and PSO optimized PSSs over Kundur's PSSs. The optimized parameters bring about the oscillations in generator speeds to settle down in a few seconds. The oscillations in optimized PSSs owing to the control effort taken by them after a disturbance settle down faster. Fig. 25 shows the tie line power flow in one of the parallel lines between buses 7 and 8. After one of the lines is permanently removed from the circuit the entire power flow is diverted

to the single path instead of two parallel paths. The oscillations in power settle down fastest for the system having optimized PSSs.

4) Operating Condition IV:

Various responses are observed for PSSs with optimized parameters for operating condition IV. The generator speed responses, corresponding PSS output and the tie-line power flow are shown in Figs. 27 to 29, respectively.

Optimized PSSs exhibit better performance than Kundur's parameters. The settling time and the overshoots in speed and tie line power are reduced when the system has optimized PSSs.
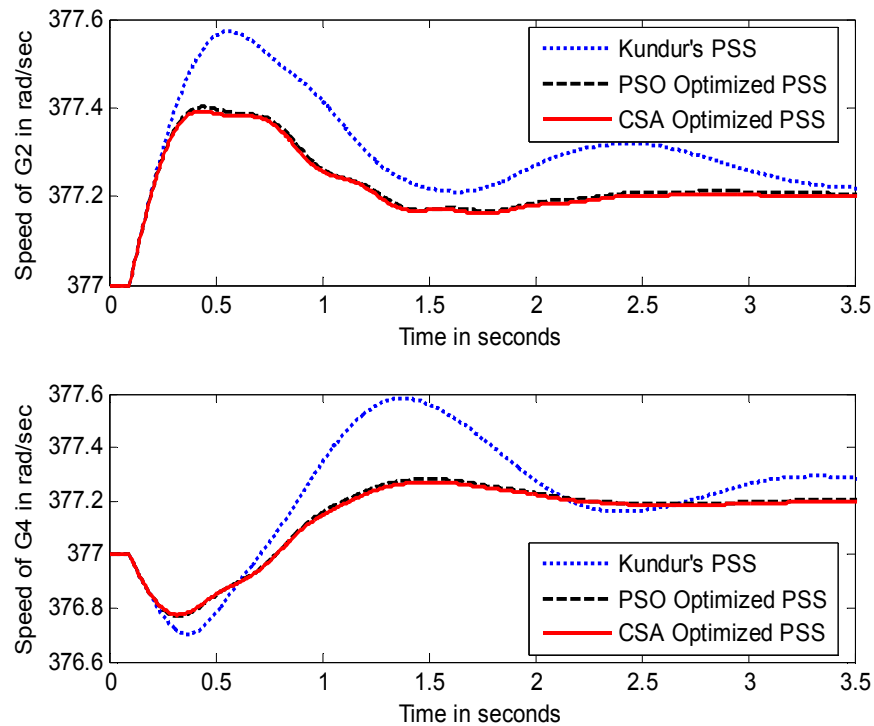
Fig. 24. Speed response of generators G2 and G4 for a permanent line outage between buses 7 and 8 for operating condition III.
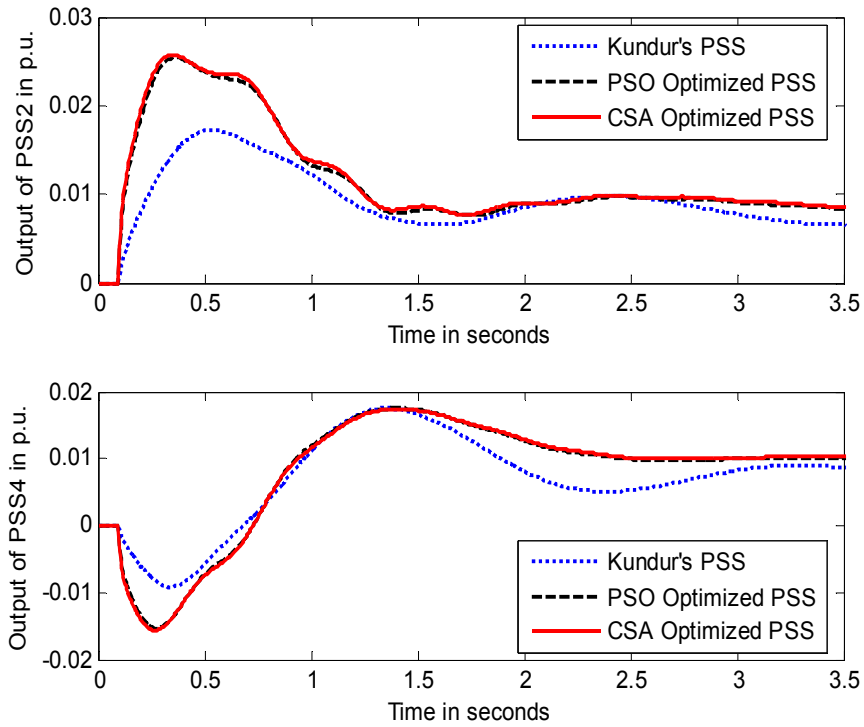
Fig. 25. Corresponding PSS outputs for PSS2 and PSS4 for a permanent line outage between buses 7 and 8 for operating condition III.
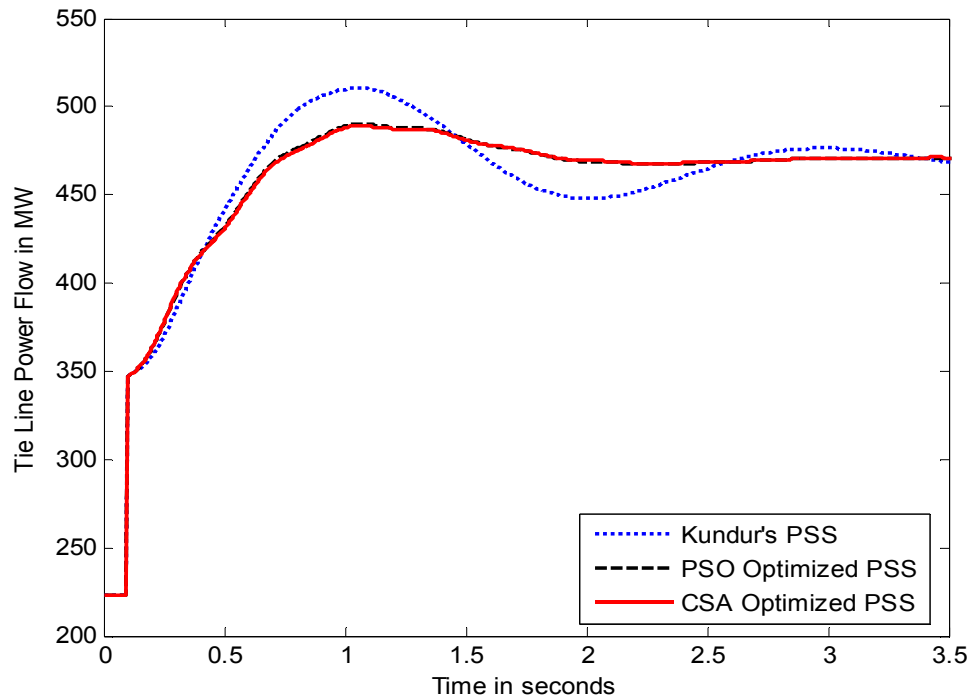
Fig. 26. Corresponding tie line power flow for a permanent line outage between buses 7 and 8 for operating condition III.
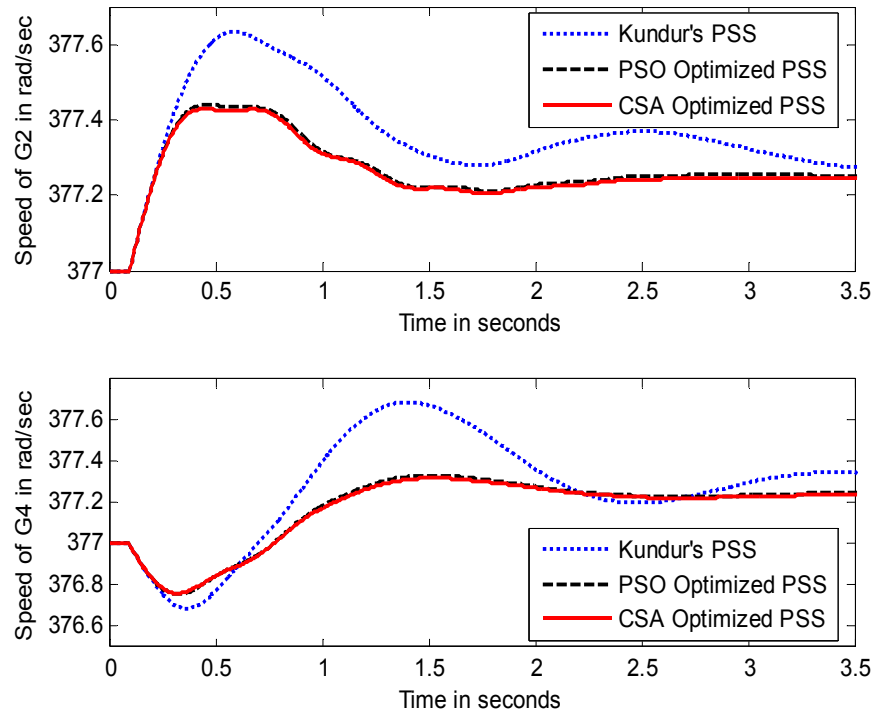
Fig. 27. Speed response of generators G2 and G4 for a permanent line outage between buses 7 and 8 for operating condition IV.
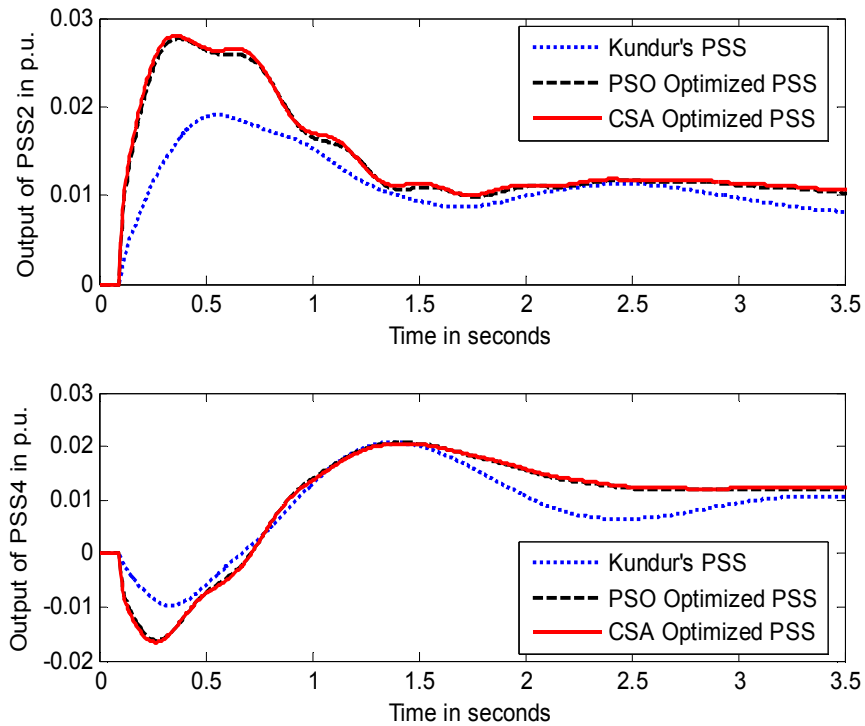
Fig. 28. Corresponding PSS outputs for PSS2 and PSS4 for a permanent line outage between buses 7 and 8 for operating condition III.
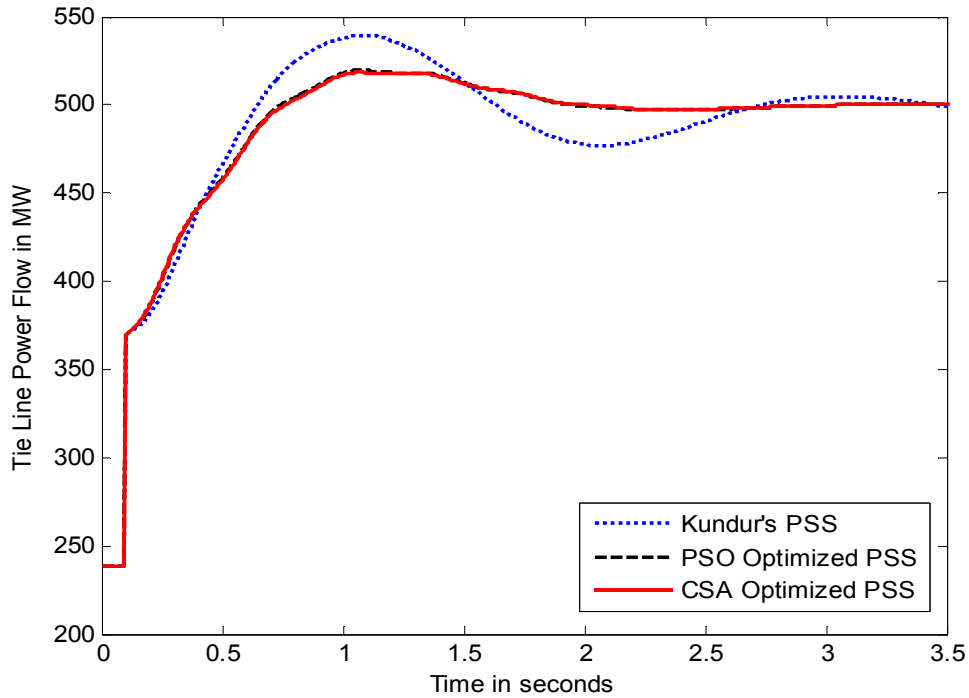
Fig. 29. Corresponding tie line power flow for a permanent line outage between buses 7 and 8 for operating condition IV.

VIII. CONCLUSION

CSA and PSO have been successfully implemented for the simultaneous design of multiple optimal PSSs for a two area power system. Both CSA and PSO optimized PSSs effectively damp out the oscillations introduced in the system. It is seen that the damping performance of CSA optimized PSS is comparable to that of PSO optimized PSS. Higher performance indices for CSA optimized PSS indicate slightly better damping performance than the PSO optimized PSS. The CSA converges faster than the PSO algorithm as it requires lesser number of fitness evaluations to converge to zero. Also, CSA is less complex computationally as compared to PSO. Hence, CSA can give better

performance than the PSO in lesser number of fitness evaluations and involving lesser computational complexities.

IX. REFERENCES

F. Rashidi, M. Rashidi, "Tuning of power system stabilizers via genetic algorithm for stabilization of power systems," 17th *Int. Conf. on Innovations in Applied Artificial Intelligence*, pp. 1210-1219, May 17-20, 2004.

H. Guo-qiang, X. Dong-jie, H. Ren-mu, "Genetic algorithm based design of power system stabilizers," *IEEE Int. Conf. on Electric Utility Deregulation, Restructuring and Power Technologies,* vol. 1, pp. 167-171, 5-8 April, 2004.

F. Rashidi, M. Rashidi, "Robust and adaptive tuning of power system stabilizers using artificial neural networks," 17th *Int. Conf. on Innovations in Applied Artificial Intelligence*, pp. 1210-1219, May 17-20, 2004.

W. Liu, G. K. Venayagamoorthy, D. C. Wunsch II, "A heuristic-dynamic based power system stailzer for a turbo-generator in a single machine power system," *IEEE Trans. On Energy Conversion,* vol. 15, pp. 297-304, Sept. 2000.

V. A. Maslennikov and S. M. Ustinov, "The optimization method for coordinated tuning of power system regulators," *Proc. on 12th Power System Computer Conf.*, PSCC, Dresden, Germany, 1996, pp. 70-75.

M. A. Abido, "A novel approach to conventional power system stabilizer design using tabu search," *Int. Journal Electric Power Energy System,* vol. 21, pp.443-454, June 1999.

M. A. Abido, "Robust design of multimachine power system using simulated annealing," *IEEE Trans. On Energy Conversion,* vol. 15, pp. 297-304, Sept. 2000.

P. Hoang, K. Tomsovic, "Design and analysis of an adaptive fuzzy power system stabilizer," *IEEE Trans. Energy Conversion*, vol. 11, no. 2, pp. 455-461, June. 1996.

M. A. Abido and Y. L. Abdel-Magid, "Optimal design of power system stabilizers using evolutionary algorithm," *IEEE Trans. on Energy Conversion,* vol. 17, no. 4, pp. 429-436, December 2002.

T. K. Das, G. K. Venayagamoorthy, "Optimal design of power system stabilizers using a small population based PSO," PES General Meeting, Montreal, Canada, June, 2006.

M. Klein, G. J. Rogers, P. Kundur, "A fundamental study of inter area oscillations in power system," IEEE Trans. on Power Systems, vol. 6, no. 3, August 1991, pp. 914-921.

P. Kundur, Power System Stability and Control, McGraw-Hill, New York: 1974, pp. 814.

F. M. Burnet, "Clonal Selection and After", Theoretical Immunology, In Bell G I, A S Perelson, G H Pimbley eds, New York, Marcel DekkerInc., 1978, pp. 63- 85.

D. Dasgupta, "Advances in Artificial Immune systems", IEEE Computational Intelligence Magazine, vol. 1, no. 4, Nov., 2006, pp. 40-49.

L. N. de Castro, F. J. Von Zuben, "Learning and Optimization Using the Clonal Selection Principle", IEEE Transactions on Evolutionary Computations, June 2002, vol. 6, no. 3, pp. 239-251.

J. Kennedy and R. Eberhart , "Particle Swarm Optimization", in Proc. IEEE Int. Conf. on Neural Networks, Perth Australia, Piscataway, NJ, IV: 1942-1948.

Y. del Valle, G. K. Venayagamoorthy, S Mohagegi, J. C. Hernandez and R. G. Harley, "Particle Swarm Optimization Basic Concepts, Variants and Applications in Power System, IEEE Trans. on Evolutionary Comp.

A. Coello Carlos and M. S. Lechuga, "MOPSO: A proposal for multiple objective particle swarm optimization," Proceedings of International Conference on Evolutionary Computation, pp. 1051-1056, 2002.

J. Kennedy, R. C. Eberhart and Y. Shi, Swarm Intelligence, Morgan Kaufmann Publishers, 2001.

PAPER 2

ARTIFICIAL IMMUNE SYSTEM BASED ALGORITHMS FOR OPTIMIZATION AND SELF-TUNING CONTROL

Mani Hunjan, *Student Member, IEEE* and

Ganesh K. Venayagamoorthy, *Senior Member, IEEE*

Abstract— **Artificial immune systems (AIS) are biologically motivated information processing systems. Several algorithms have been inspired by various mechanisms of the biological immune system. The clonal selection mechanism of the immune system is a powerful optimization and recognition technique. This paper presents optimization results on four benchmark functions and the design of an optimal excitation controller (OEC) for a generator on an electric ship. Clonal selection algorithm (CSA) produces better solutions and has fast convergence. The concept of adaptive immunity in biological immune systems is extended for the design of a self-tuning optimal excitation controller (STOEC) to handle high energy loads on an electric ship such as electric guns, electromechanical aircraft launchers, high power sensors, and directed energy weapons. The STOEC can effectively control the output voltage and the reactive power of the generator during pulsed loads, stabilizing the terminal voltage quickly with minimal speed deviations. The STOEC considerably reduces the field current overshoot and minimizes power losses in the field circuit. Simulation results are provided to compare the performance of the conventional controller and the STOEC.**

Index Terms -- **Adaptive immunity, artificial immune system, clonal selection algorithm, excitation control, immune feedback law, pulsed loads.**

I. INTRODUCTION

Artificial immune systems (AIS) are inspired by the principles and processes of the immune system. AIS algorithms typically exploit the immune systems characteristics of learning and memory. Its learning takes place by evolutionary processes. Processes in AIS which are investigated and simulated are clonal selection for B cells [1], negative selection of T cells [2], affinity maturation [3] and immune network theory [4]. AIS have been applied to areas such as optimization [5], robotic systems [6], machine learning [7], network intrusion detection [8], anomaly detection [9], fault diagnosis [10], scheduling [11], computer security [12], data analysis [13], and many other areas.

Clonal selection algorithm (CSA) is based on the principles of clonal selection and affinity maturation of the biological immune system. Clonal selection principle explains how an immune response is mounted when an antigen is recognized. It is based on a principle that only certain cells are selected for destruction of specific antigens. The fundamental concept of CSA is that only the cells that recognize the intruding antigen are selected for cloning. CSA has been increasingly used in various areas of engineering and research, including applications in pattern recognition [14], machine learning [15] and multi-modal optimization [16].

In this paper, two studies are carried out using CSA. It is first used for optimization of four benchmark functions and the results are compared with those

obtained using genetic algorithm (GA) and particle swarm optimization (PSO). CSA is then used for the design of an optimal excitation controller (OEC) for a future electric ship. Further, CSA and adaptive immune algorithm are used in the design of a self-tuning optimal excitation controller (STOEC), to specifically handle pulsed loads on the ship.

Future electric ship power system design should be reliable and survivable [17]. It should be able to support new systems that require pulse power levels which are two to three times the magnitude of the total power installed onboard the ship. An efficient method is required for voltage control of the generator especially during pulsed loads to maintain power continuity and regulation. Arcidiacono *et al.* proposed a concept of a shipboard integrated voltage and VAR control method to fulfill the power quality requirements of the electric ship in [18]. The pulsed-power loads on an electric ship like electric launchers, electric guns, high power sensors, and directed energy weapons cause variations in the power demand. During pulsed power load demand there is a small drop in the turbine speed and large oscillations are introduced in the generator terminal voltage and the propulsion motor speed [19]. The challenge is to provide power continuity and regulation after firing of these high energy weapons [20]. The oscillations in the terminal voltage are of primary concern for the electric ship power system under pulsed load conditions. Hence, a nonlinear controller is required for controlling the terminal voltage of the generator and damping out any oscillations in the system.

This paper is organized as follows: Section II describes the biological immune system; Section III describes the CSA used for optimization; Section IV deals with optimization of four benchmark functions; Section V discusses the electric ship excitation system and explains the design of an immune system based STOEC; Section VI presents

simulation results for the immune system based STOEC. Finally, the conclusions and future work are given in Section VII.

II. BACKGROUND ON BIOLOGICAL IMMUNE SYSTEM

The artificial immune system is a biologically motivated information processing system. It is a parallel and distributive adaptive system which can learn new information, recall previously learned information and perform pattern recognition tasks in a decentralized fashion. Its learning takes place by evolutionary processes. The powerful information processing capabilities of the immune system, such as feature extraction, pattern recognition, learning, memory and its distributive nature provide metaphors for its artificial counterpart [21]. The immune system involves various mechanisms and among them a few have been investigated and simulated. These include immune network models [22], clonal selection principle [23], and negative selection algorithms [24]. The main role of the immune system is to recognize all cells within the body and categorize them as self or non-self. The non-self cells are further categorized in order to induce an appropriate type of defense mechanism.

The immune system has two types of responses: innate and adaptive. Innate immunity is a non specific defense mechanism. The adaptive immunity is antigen specific and adapts to previously unseen molecule. Unlike the innate immune response, it becomes more efficient on subsequent exposure to the same antigen. When the antigens penetrate the epithelial surface, they encounter cells and molecules that mount an innate immune response. Macrophages conduct defense by means of surface receptors that

recognize and bind to common constituents of antigen surfaces and engulf the antigen. Antigens are also ingested by the immature dendritic cell in the infected tissue. Binding of antigen to the receptor stimulates the dendritic cell to engulf the antigen and degrade it intracellularly. On activation, the dendritic cells mature into highly effective antigen presenting cell (APC) and in turn activate antigen specific lymphocytes (B cells and T cells). Lymphocytes bear antigen receptors of a single specificity and are responsible for the adaptive immune response of the human body.

Adaptive immune response is realized by the interplay of various cells in the body. Among these cells, the T-cells and the B-cells play the most important roles. B-cells can secrete antibodies and can perform the nonspecific humoral immunity. T-cells are comprised of three subsets; the helper T-cells (T_H), the suppressor T-cells (T_S) and the killer T-cells (T_C). The function of the T-cells is to adjust the immune process and remove antigens. For adjustment, the T-cells improve and enhance the immune response on appearance of an antigen, and inhibit the reproduction of immune cells to restore dynamic balance of the system once the number of antigen falls below a certain limit. Killer T-cells secrete cytotoxin to kill antigens and perform specific cell-mediated immunity [22].

The immune system exhibits two types of responses: T cell mediated cell immune response and B cell mediated humoral immune response. For humoral immune response, the antigen presenting cell (APC) captures the antigen and activates CD4+T cells which clone and differentiate into the T_S (suppressor) and T_H (helper) cells. APC are highly specialized cells that can process antigens and present them for T cell activation. The T_H cells activate the B cells which capture the antigen. The B cells are activated both by the antigen itself and T cells. T_S cells suppress the action of T_H cells at later stage [25].

The flowchart in Fig. 1 shows innate and B-cell mediated humoral immune response to the presence of antigens in the human body. Stages 1 and 2 correspond to the innate immune response and the B-cell based adaptive immune response, respectively.
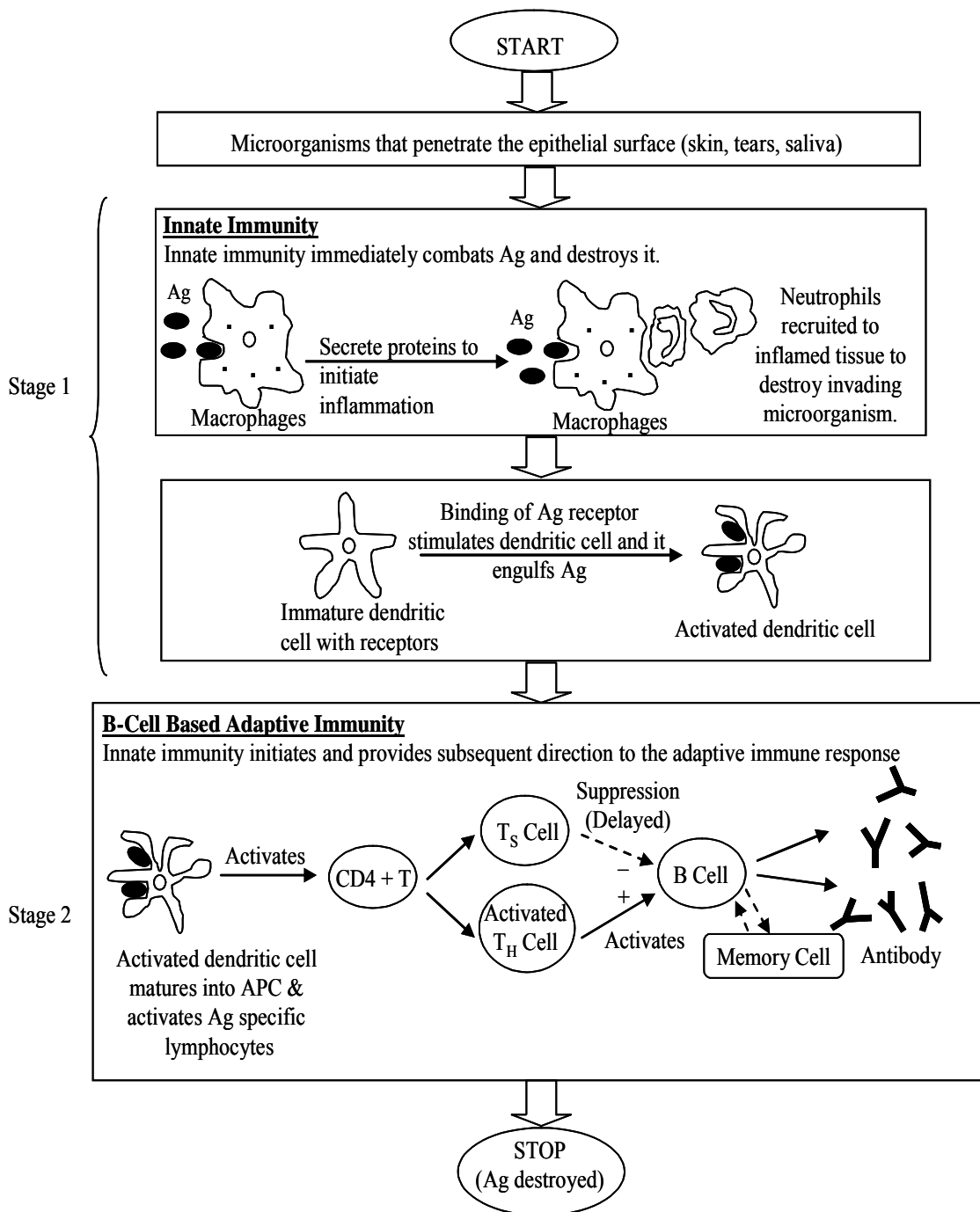
Fig. 1. Overview of innate immune and B-cell mediated adaptive immune response.

Within the immune system, there is a feedback mechanism which simultaneously performs two diverse tasks: rapidly responding to the presence of foreign material while quickly stabilizing the immune system. This feedback mechanism involves cooperation between the inhibitive mechanism (T_S cells) and the main feedback mechanism. The activation of B-cells in response to antigens is the main feedback mechanism of the immune system. The suppressor T-cells and the foreign materials activate the suppressor T-cells, and the suppressor T-cells inhibits the activities of all other cells. As a result the reaction of the immune system is subdued. This is the inhibitive mechanism [25].

III. CLONAL SELECTION ALGORITHM

The core of the adaptive immune response is the clonal selection principle or the clonal selection theory. The clonal selection theory was introduced by F. M. Burnet in 1958 [26]. The clonal selection principle describes response of the immune system to antigens [21]. Its principle is based on the fact that only certain B and T cells are selected for destruction of specific antigens invading the body. When B and T cells encounter antigens, they are activated to produce antibody molecules. Each B and T cell can produce only one kind of specific antibody molecule capable of recognizing and binding to this specific antigen. And it is this binding that stimulates the B cell to reproduce itself one or more times and later differentiate into plasma cells. This asexual proliferation generates daughter cells or clone cells. Therefore, only those cells that recognize the antigen proliferate, thus being selected against those that do not. The main features of the current clonal selection theory are that:

- Stimulation of certain B and T cells by antigens causes proliferation and differentiation.

- Non-stimulated cells are suppressed.

- The new cells generated are mutated clones of the parents (affinity maturation) representing a generation with random genetic changes. The mutation rate is proportional to the cell affinity.

- Newly differentiated lymphocytes which carry self-reactive or low-affinity antigenic receptors are eliminated.

Clonal selection principle or algorithm has been applied in pattern recognition and optimization problems. The clonal selection algorithm basically consists of two populations; a set of antigens (*Ag*) and a set of antibodies (*Ab*). The basic CSA [27] is modified in this paper by mutating the cloned population such that the new set of antibodies generated after maturation drive the algorithm towards the global optimum. The modified CSA used for optimization is described as follows and its flowchart is depicted in Fig. 2.

1) Randomly generate a population of *N* antibodies.

2) Determine affinity of *Ag* to all the *N* antibodies. For optimization problems the affinity could be directly proportional or inversely proportional to the objective function that needs to be maximized or minimized, respectively.

3) Select *C* antibodies with highest affinity (C<N).

4) Clone the *C* selected antibodies. The number of clones generated for each of the antibodies can be given by
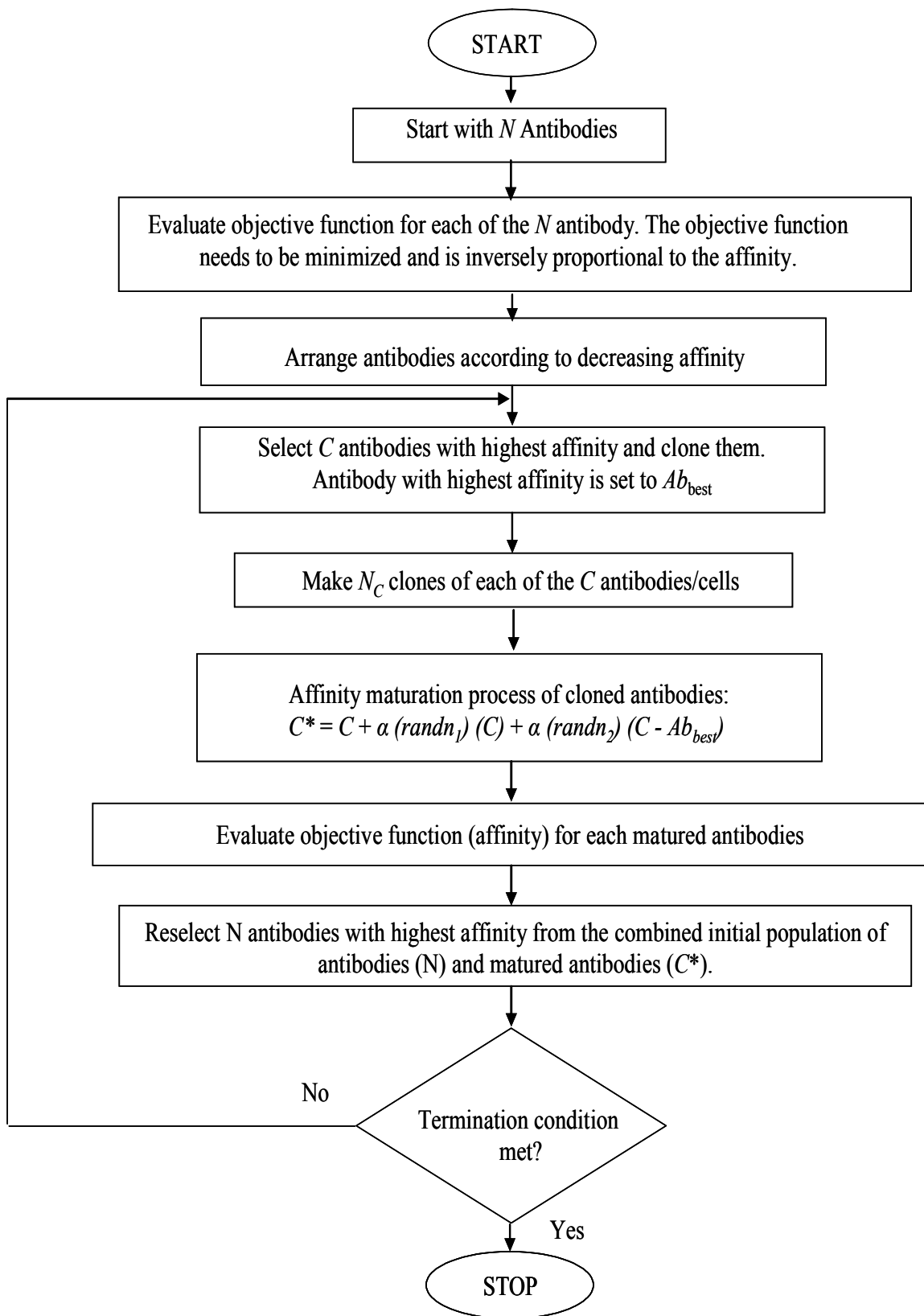
Fig. 2. Flowchart for the modified clonal selection algorithm.

$$N_c = round(\beta.N) \tag{1}$$

where N_c is number of clones generated for each antibody, β is a multiplying factor, N is the total number of antibodies, and round ( ) is an operator which rounds its argument to the closest integer.

5) Store the antibody with the greatest affinity as Ab_{best}.

6) The cloned set of antibodies next undergoes affinity maturation. This affinity maturation is inversely proportional to the antigenic affinity. The higher the antigenic affinity, the lower the mutation rate. The affinity maturation of the cloned antibodies is calculated using

$$C^* = C + \alpha(rand_1)C + \alpha(rand_2)(C - Ab_{best}) \tag{2}$$

where C^* is the set of population obtained after cloning and affinity maturation of the C antibodies, α is calculated using

$$\alpha = \exp(-f) \tag{3}$$

where f is the normalized fitness or objective function of the antibody being mutated. $rand_1$ and $rand_2$ are random numbers in a uniform distribution between 0 and 1. The affinity maturation of the cloned antibodies tends to drive the next set of antibodies towards the global optimum by taking into consideration the antibody with the greatest affinity (Ab_{best}).

7) Determine the antigenic affinity of the matured antibodies. Reselect N antibodies with the highest affinity and repeat step 3 until some termination condition is satisfied.

The modified CSA summarized above is used for optimization of benchmark functions and to determine the parameters of the OEC. The modified CSA is also used to

determine optimal values of certain parameters required to apply the adaptive immune algorithm for self-tuning of the OEC on the electric ship during pulsed loads.

IV. CSA OPTIMIZATION OF BENCHMARK FUNCTIONS

Four nonlinear benchmark functions are optimized using CSA. The optimization results are compared with those obtained using GA and PSO. These four benchmark functions are given in (4)-(7).

Sphere:

$$f_0(x) = \sum_{i=1}^{n} x_i^2 \tag{4}$$

Rosenbrock:

$$f_1(x) = \sum_{i=1}^{n} (100(x_{i+1} - x_i^2)^2 + (x_i - 1)^2) \tag{5}$$

Rastrigrin:

$$f_2(x) = \sum_{i=1}^{n} (x_i^2 - 10 \cos(2\pi x_i) + 10) \tag{6}$$

Griewank:

$$f_{3(x)} = \frac{1}{4000} \sum_{i=1}^{n} x_i^2 - \prod_{i=1}^{n} \cos(\frac{x_i}{\sqrt{i}}) + 1 \tag{7}$$

Among the four functions given above, the Sphere and Rosenbrock are unimodal functions while the Griewank and Rastrigrin are multimodal functions. For comparison purposes, the asymmetric initialization method is used for population initialization [28]. The initialization ranges for these four functions are listed in Table I.

Table I

Asymmetric Initialization Ranges for the Benchmark Functions

f_0	(50, 100)
f_1	(15, 30)
f_2	(2.56, 5.12)
f_3	(300, 600)

The different optimization techniques are compared for various dimension and population sizes. The different dimension sizes are 10, 20, 30, 50, 100 and the corresponding maximum number of generations was set to 1000, 1500, 2000, 3000, and 5000. Different population sizes of 20, 50 and 100 are investigated for each function. The average over 50 trials is taken for each experimental setting when determining the mean fitness value. Tables II-IV list the mean fitness and standard deviation (std) of the best particle/chromosome/antibody obtained for the four benchmark functions for population sizes of 20, 50 and 100, respectively. It is seen that CSA has the ability to produce better solutions and converges quickly compared to PSO and GA on different dimensions and population sizes. A CSA with hyper mutation and spatial clone extension (HSCSA) was proposed in [29], and used for optimization of the benchmark functions. The results obtained for these benchmark functions using HSCSA [29] are also included for comparison purposes (population size of 50 and dimensions of 10, 20 and 30). The optimization results for the basic clonal selection algorithm (BCSA) have also been included [29]. It is seen that the modified CSA outperforms HSCSA and BCSA as it uses lesser number of iterations. This can mainly be attributed to the affinity maturation process employed, given by (2).

The next section describes the design of a STOEC using CSA for finding the optimal controller parameters and B cell mediated adaptive immune response for incorporation of self-tuning characteristics to the optimal controller.

Table II

Mean Fitness and Standard Deviation of Benchmark Functions for Population Size of 20

Algorithm	Dimension	Iteration	Sphere Mean Fitness ± std	Rosenbrock Mean Fitness ± std	Rastrigrin Mean Fitness ± std	Griewank Mean Fitness ± std
PSO	10	1000	4.8033×10^{-20} $\pm 1.3087 \times 10^{-19}$	5.7796×10^{1} $\pm 8.3621 \times 10^{1}$	5.9283×10^{0} $\pm 2.5418 \times 10^{0}$	8.8601×10^{-2} $\pm 5.4193 \times 10^{-2}$
GA	10	1000	5.6574×10^{-1} $\pm 1.2474 \times 10^{-1}$	1.8123×10^{2} $\pm 5.9371 \times 10^{1}$	1.4503×10^{2} $\pm 1.6453 \times 10^{1}$	1.3178×10^{1} $\pm 3.2287 \times 10^{0}$
CSA	**10**	**1000**	$\mathbf{2.2428 \times 10^{-286}}$ $\mathbf{\pm 0}$	$\mathbf{2.8000 \times 10^{-3}}$ $\mathbf{\pm 2.5000 \times 10^{-3}}$	**0** $\mathbf{\pm 0}$	$\mathbf{7.6000 \times 10^{-3}}$ $\mathbf{\pm 2.2600 \times 10^{-2}}$
PSO	20	1500	6.3389×10^{-11} $\pm 1.9160 \times 10^{-10}$	9.2408×10^{2} $\pm 8.2693 \times 10^{2}$	1.7659×10^{1} $\pm 8.5221 \times 10^{0}$	2.6633×10^{-2} $\pm 2.2523 \times 10^{-2}$
GA	20	1500	2.3509×10^{0} $\pm 2.8241 \times 10^{-1}$	7.1724×10^{2} $\pm 1.1305 \times 10^{2}$	4.2243×10^{2} $\pm 2.9855 \times 10^{1}$	5.3278×10^{1} $\pm 5.7485 \times 10^{0}$
CSA	**20**	**1500**	$\mathbf{3.1030 \times 10^{-286}}$ $\mathbf{\pm 0}$	$\mathbf{1.8000 \times 10^{-3}}$ $\mathbf{\pm 1.5000 \times 10^{-3}}$	**0** $\mathbf{\pm 0}$	$\mathbf{2.5000 \times 10^{-3}}$ $\mathbf{\pm 7.000 \times 10^{-3}}$
PSO	30	2000	1.6127×10^{-7} $\pm 3.3811 \times 10^{-6}$	4.4499×10^{3} $\pm 6.2317 \times 10^{2}$	5.3551×10^{1} $\pm 1.6669 \times 10^{1}$	1.6832×10^{-2} $\pm 1.3945 \times 10^{-2}$
GA	30	2000	4.4996×10^{0} $\pm 3.9461 \times 10^{-1}$	1.4368×10^{3} $\pm 1.7801 \times 10^{2}$	7.3898×10^{2} $\pm 3.9557 \times 10^{1}$	1.0344×10^{2} $\pm 1.0329 \times 10^{1}$
CSA	**30**	**2000**	$\mathbf{6.9986 \times 10^{-316}}$ $\mathbf{\pm 0}$	$\mathbf{1.2000 \times 10^{-3}}$ $\mathbf{\pm 1.1000 \times 10^{-3}}$	**0** $\mathbf{\pm 0}$	$\mathbf{3.1321 \times 10^{-3}}$ $\mathbf{\pm 1.1667 \times 10^{-2}}$
PSO	50	3000	1.3000×10^{-3} $\pm 2.0000 \times 10^{-3}$	1.7965×10^{4} $\pm 1.0326 \times 10^{4}$	1.6893×10^{2} $\pm 3.8124 \times 10^{1}$	1.0054×10^{-2} $\pm 8.6159 \times 10^{-3}$

Table II (Cont'd)

Mean Fitness and Standard Deviation of Benchmark Functions for Population Size of 20

Algorithm	Dimension	Iteration	Sphere Mean Fitness ± std	Rosenbrock Mean Fitness ± std	Rastrigrin Mean Fitness ± std	Griewank Mean Fitness ± std
GA	50	3000	8.9625×10^{0} $\pm 6.2765 \times 10^{-1}$	3.0757×10^{3} $\pm 3.9806 \times 10^{2}$	1.3828×10^{3} $\pm 3.8634 \times 10^{1}$	2.1476×10^{2} $\pm 1.5087 \times 10^{1}$
CSA	50	3000	**0** **±0**	**5.7920×10^{-4}** **$\pm 1.8670 \times 10^{-4}$**	**0** **±0**	**5.1774×10^{-3}** **$\pm 1.5698 \times 10^{-2}$**
PSO	100	5000	7.7553×10^{1} $\pm 9.8366 \times 10^{1}$	6.2672×10^{4} $\pm 3.8911 \times 10^{4}$	4.5969×10^{2} $\pm 1.0011 \times 10^{2}$	1.3142×10^{1} $\pm 6.0771 \times 10^{1}$
GA	100	5000	8.2252×10^{1} $\pm 8.7782 \times 10^{-1}$	7.9183×10^{3} $\pm 9.1288 \times 10^{2}$	3.1676×10^{3} $\pm 4.7413 \times 10^{1}$	5.2221×10^{2} $\pm 2.3425 \times 10^{1}$
CSA	100	5000	**0** **±0**	**5.4856×10^{-4}** **$\pm 4.9652 \times 10^{-4}$**	**0** **±0**	**4.7179×10^{-3}** **$\pm 1.2532 \times 10^{-2}$**

Table III

Mean Fitness and Standard Deviation of Benchmark Functions for Population Size of 50

Algorithm	Dimension	Iteration	Sphere Mean Fitness ± std	Rosenbrock Mean Fitness ± std	Rastrigrin Mean Fitness ± std	Griewank Mean Fitness ± std
PSO	10	1000	5.0737×10^{-25} $\pm 1.9522 \times 10^{-24}$	5.7759×10^{0} $\pm 6.6032 \times 10^{0}$	1.5199×10^{0} $\pm 2.2732 \times 10^{0}$	8.3646×10^{-2} $\pm 3.7839 \times 10^{-2}$
GA	10	1000	5.3100×10^{-1} $\pm 1.0466 \times 10^{-1}$	1.9413×10^{2} $\pm 3.6323 \times 10^{1}$	1.5307×10^{2} $\pm 1.0652 \times 10^{1}$	1.2872×10^{2} $\pm 2.8169 \times 10^{1}$
CSA	10	1000	**0** **±0**	**1.7895×10^{-4}** **$\pm 1.6158 \times 10^{-4}$**	**0** **±0**	**2.3716×10^{-3}** **$\pm 8.0469 \times 10^{-3}$**
BCSA[1]	10	10000	7.0×10^{-12}	5.6×10^{-1}	3.98×10^{0}	2.99×10^{-2}
HSCSA[1]	10	10000	6.0×10^{-13}	3.7×10^{-4}	1.17×10^{-12}	7.4×10^{-3}
PSO	20	1500	1.2006×10^{-15} $\pm 2.2215 \times 10^{-15}$	5.1767×10^{1} $\pm 4.3075 \times 10^{1}$	1.5224×10^{1} $\pm 7.1939 \times 10^{0}$	3.1701×10^{-2} $\pm 3.1166 \times 10^{-2}$

[1] Z. Jin and *et al.* [29].

Table III (Cont'd)

Mean Fitness and Standard Deviation of Benchmark Functions for Population Size of 50

Algorithm	Dimen-sion	Itera-tion	Sphere Mean Fitness ± std	Rosenbrock Mean Fitness ± std	Rastrigrin Mean Fitness ± std	Griewank Mean Fitness ± std
GA	20	1500	2.3831×10^{0} $\pm 2.1856 \times 10^{-1}$	8.2558×10^{2} $\pm 1.3281 \times 10^{2}$	4.1778×10^{2} $\pm 3.8515 \times 10^{1}$	5.3097×10^{1} $\pm 6.0004 \times 10^{0}$
CSA	20	1500	**0** **±0**	**5.6090×10^{-5}** **$\pm 5.9619 \times 10^{-5}$**	**0** **±0**	**3.4058×10^{-3}** **$\pm 1.2112 \times 10^{-2}$**
BCSA[1]	20	10000	2.0×10^{-12}	1.34×10^{1}	5.17×10^{1}	1.24×10^{-2}
HSCSA[1]	20	10000	1.6×10^{-13}	2.61×10^{-2}	1.1×10^{-3}	5.1×10^{-5}
PSO	30	2000	4.3010×10^{-11} $\pm 7.0211 \times 10^{-11}$	1.7598×10^{2} $\pm 8.2477 \times 10^{1}$	4.4744×10^{1} $\pm 9.3397 \times 10^{0}$	1.0923×10^{-2} $\pm 1.3808 \times 10^{-2}$
GA	30	2000	4.3167×10^{0} $\pm 4.9075 \times 10^{-1}$	1.8555×10^{3} $\pm 2.5339 \times 10^{2}$	7.2126×10^{2} $\pm 3.5999 \times 10^{1}$	1.0099×10^{1} $\pm 1.1251 \times 10^{0}$
CSA	30	2000	**0** **±0**	**5.7026×10^{-5}** **$\pm 5.2079 \times 10^{-5}$**	**0** **±0**	**2.7838×10^{-3}** **$\pm 1.0917 \times 10^{-2}$**
BCSA[1]	30	10000	1.0×10^{-13}	2.68×10^{1}	1.13×10^{2}	4.31×10^{-2}
HSCSA[1]	30	10000	7.8×10^{-14}	4.29×10^{-2}	4.15×10^{-2}	4.5×10^{-3}
PSO	50	3000	1.2003×10^{-6} $\pm 1.6389 \times 10^{-6}$	6.8001×10^{2} $\pm 3.1901 \times 10^{2}$	1.2101×10^{2} $\pm 2.7912 \times 10^{1}$	6.8409×10^{-3} $\pm 1.2508 \times 10^{-2}$
GA	50	3000	9.4004×10^{0} $\pm 4.4393 \times 10^{-1}$	4.0580×10^{3} $\pm 3.5573 \times 10^{2}$	1.3579×10^{3} $\pm 7.9975 \times 10^{1}$	2.1599×10^{2} $\pm 1.3498 \times 10^{1}$
CSA	50	3000	**0** **±0**	**3.9769×10^{-5}** **$\pm 3.5195 \times 10^{-5}$**	**0** **±0**	**3.4979×10^{-3}** **$\pm 1.0304 \times 10^{-2}$**
PSO	100	5000	2.0013×10^{0} $\pm 3.6837 \times 10^{0}$	2.5941×10^{3} $\pm 1.2979 \times 10^{3}$	4.3674×10^{2} $\pm 7.5984 \times 10^{1}$	3.5858×10^{-1} $\pm 2.5273 \times 10^{-1}$
GA	100	5000	2.2408×10^{1} $\pm 6.6576 \times 10^{-1}$	1.0960×10^{4} $\pm 9.2866 \times 10^{2}$	3.2118×10^{3} $\pm 6.5126 \times 10^{1}$	5.2086×10^{2} $\pm 1.6781 \times 10^{1}$
CSA	100	5000	**0** **±0**	**2.2812×10^{-5}** **$\pm 2.0096 \times 10^{-5}$**	**0** **±0**	**4.6971×10^{-3}** **$\pm 1.5765 \times 10^{-2}$**

Table IV

Mean Fitness and Standard Deviation of Benchmark Functions for Population Size of 100

Algorithm	Dimen-sion	Itera-tion	Sphere Mean Fitness ± std	Rosenbrock Mean Fitness ± std	Rastrigrin Mean Fitness ± std	Griewank Mean Fitness ± std
PSO	10	1000	8.5348×10^{-29} $\pm 5.0570 \times 10^{-28}$	1.5612×10^{0} $\pm 1.8106 \times 10^{0}$	1.2231×10^{0} $\pm 1.3642 \times 10^{0}$	6.7407×10^{-2} $\pm 2.5794 \times 10^{-2}$
GA	10	1000	5.2071×10^{-1} $\pm 1.3566 \times 10^{-1}$	1.7357×10^{2} $\pm 5.3820 \times 10^{1}$	1.4001×10^{2} $\pm 1.7217 \times 10^{1}$	1.3544×10^{1} $\pm 2.4211 \times 10^{0}$
CSA	10	1000	**0** **±0**	**5.5294×10^{-5}** **$\pm 5.2602 \times 10^{-5}$**	**0** **±0**	**4.4581×10^{-4}** **$\pm 3.1524 \times 10^{-3}$**
PSO	20	1500	1.4092×10^{-18} $\pm 5.2892 \times 10^{-18}$	2.5588×10^{1} $\pm 2.5075 \times 10^{1}$	1.4125×10^{1} $\pm 2.5415 \times 10^{1}$	2.1241×10^{-2} $\pm 1.8943 \times 10^{-2}$
GA	20	1500	2.2214×10^{0} $\pm 3.8605 \times 10^{-1}$	8.5984×10^{2} $\pm 1.3753 \times 10^{2}$	$4.1865 x 10^{2}$ $\pm 3.0812 \times 10^{1}$	5.4517×10^{1} $\pm 6.4885 \times 10^{0}$
CSA	20	1500	**0** **±0**	**3.2367×10^{-5}** **$\pm 3.1744 \times 10^{-5}$**	**0** **±0**	**3.5174×10^{-4}** **$\pm 2.4872 \times 10^{-3}$**
PSO	30	2000	1.0552×10^{-13} $\pm 2.5525 \times 10^{-13}$	4.1822×10^{2} $\pm 2.4237 \times 10^{2}$	3.5789×10^{1} $\pm 9.2777 \times 10^{0}$	1.8751×10^{-2} $\pm 1.6103 \times 10^{-2}$
GA	30	2000	4.2358×10^{0} $\pm 5.3582 \times 10^{-1}$	1.8183×10^{3} $\pm 2.0197 \times 10^{2}$	7.0274×10^{2} $\pm 4.1394 \times 10^{1}$	1.0757×10^{2} $\pm 8.5052 \times 10^{0}$
CSA	30	2000	**0** **±0**	**2.3533×10^{-5}** **$\pm 2.2122 \times 10^{-5}$**	**0** **±0**	**6.0015×10^{-4}** **$\pm 3.0128 \times 10^{-3}$**
PSO	50	3000	8.0544×10^{-9} $\pm 1.0295 \times 10^{-8}$	1.4132×10^{2} $\pm 4.5161 \times 10^{1}$	1.0081×10^{2} $\pm 1.3302 \times 10^{1}$	8.4013×10^{-3} $\pm 1.3877 \times 10^{-2}$
GA	50	3000	9.0765×10^{0} $\pm 6.4170 \times 10^{-1}$	4.1657×10^{3} $\pm 2.9128 \times 10^{2}$	1.3562×10^{3} $\pm 6.1185 \times 10^{1}$	2.0651×10^{3} $\pm 8.8780 \times 10^{0}$
CSA	50	3000	**0** **±0**	**1.6198×10^{-5}** **$\pm 1.6649 \times 10^{-5}$**	**0** **±0**	**0** **±0**
PSO	100	5000	1.2031×10^{-1} $\pm 4.2129 \times 10^{-1}$	3.0276×10^{2} $\pm 1.0954 \times 10^{2}$	4.2378×10^{2} $\pm 7.0073 \times 10^{1}$	1.9960×10^{-2} $\pm 1.7102 \times 10^{-2}$

Table IV (Cont'd)

Mean Fitness and Standard Deviation of Benchmark Functions for Population Size of 100

Algorithm	Dimension	Iteration	Sphere Mean Fitness ± std	Rosenbrock Mean Fitness ± std	Rastrigrin Mean Fitness ± std	Griewank Mean Fitness ± std
GA	100	5000	2.2930×10^1 $\pm 9.3424 \times 10^{-1}$	1.1534×10^4 $\pm 4.9472 \times 10^2$	3.1596×10^3 $\pm 1.4033 \times 10^2$	5.1611×10^2 $\pm 2.1046 \times 10^1$
CSA	100	5000	**0** **±0**	**8.5441×10^{-6}** **$\pm 8.1335 \times 10^{-6}$**	**0** **±0**	**0** **±0**

V. ELECTRIC SHIP EXCITATION CONTROLLER DESIGN

The Navy's planned DD(X) shipboard power system has four gas turbine-generator sets, two main and two auxiliary [20]. Fig. 3 shows a typical generation and AC propulsion motor shipboard power system setup. The pulsed loads are connected to the three phase distribution bus of the system. A number of researchers have investigated the pulsed power requirements for the electromagnetic weapons and sensors and impact of pulse power loads on the naval power and the ship propulsion systems [30]. This pulse energy demand has to be provided by the ship energy sources, while not impacting the operation of the rest of the system.

The exciter with a conventional excitation controller is shown in Fig. 3. The excitation system is a IEEE Static excitation system # 1   (STA1) [31], where, E_{FD} is the exciter output voltage, I_{LR} is the exciter output current limit reference, I_{FD} is limiter gain and V_T is the generator terminal voltage. The values of the parameters of the excitation system are given in Table B.1 in the Appendix [32].
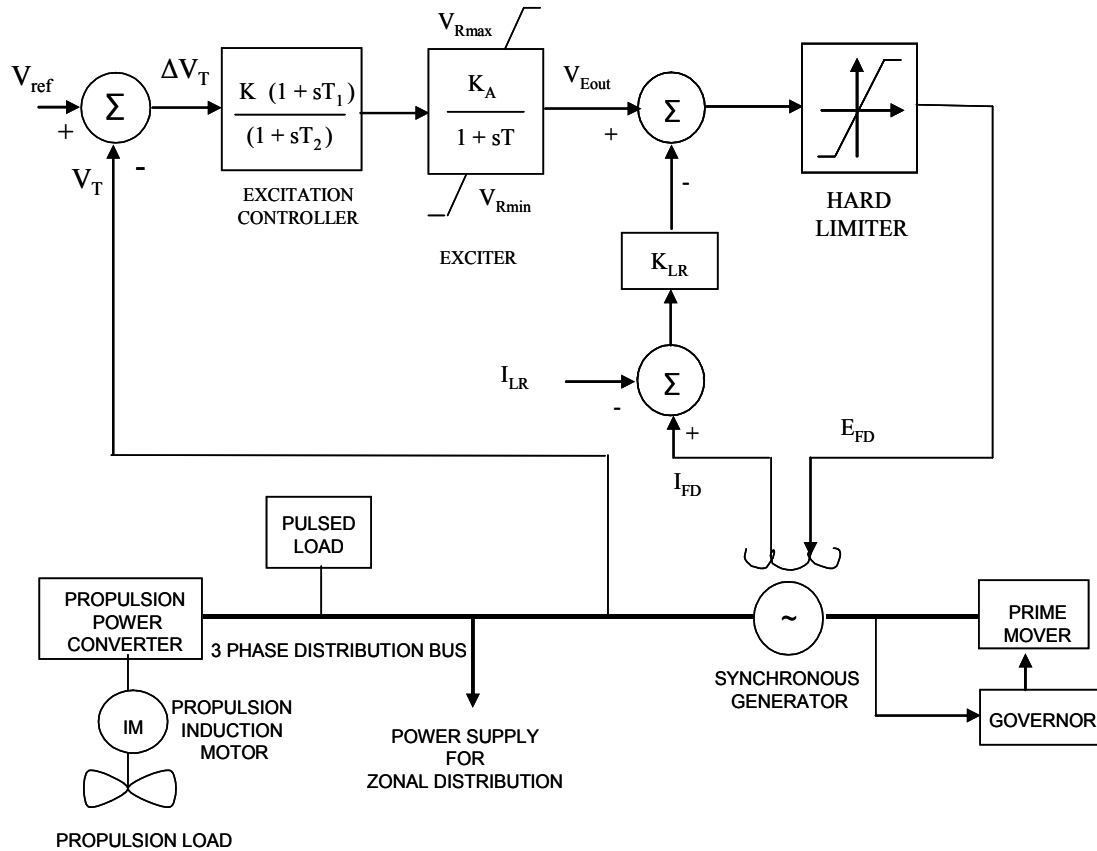
Fig. 3. Generation-AC propulsion motor shipboard power system.

The excitation controller has three parameters; the gain constant (K), and two time constants (T_1 and T_2). The optimal values of these parameters are found using modified CSA. The concept of the immune feedback mechanism is then applied to this OEC to obtain the STOEC. The flowchart in Fig. 4 illustrates the entire steps involved in the realization of the STOEC.

The realization of STOEC basically involves design and operation phases as explained in the following subsections. The design of the OEC system corresponds to innate immunity i.e. stage 1 and adaptation of OEC parameters using immune feedback

START

Initialization of excitation controller parameters (K, T_1, T_2)

Optimal Excitation Controller

Controller Parameters (K, T_1, T_2)

Simulations of the electric ship power system (PSCAD/EMTDC Software)

Stage 1

Iterations

Termination criterion met?

No

Optimal excitation controller parameters determined using modified CSA

Yes → STOP

Optimal excitation controller parameters

Initialization of AIS parameters m_1 to m_6

Self-Tuning Controller

AIS Parameters (m_1 to m_6)

Simulations of the electric ship power system (PSCAD/EMTDC Software)

Stage 2

Iterations

Termination criterion met?

No

Optimal values of AIS parameters determined using modified CSA

Yes → STOP

Design Phase

Optimal m_1 to m_6

Self-Tuning Optimal Excitation Controller

Adaptation of excitation controller parameters (K, T_1, and T_2) based on immune feedback law.

$$K(k) = K + \left[m_1 - m_2 \left\{ \exp\left(-\left(\frac{\Delta V_T(k)}{\Delta V_T(k-1)} \right)^2 \right) \right\} \right] \Delta V_T(k)$$

$$T_i(k) = T_i + \left[m_{1+2i} - m_{2+2i} \left\{ \exp\left(-\left(\frac{\Delta V_T(k)}{\Delta V_T(k-1)} \right)^2 \right) \right\} \right] \Delta V_T(k)$$

$i=1, 2$

Operation Phase

STOP

Fig. 4. Flowchart illustrating design and operation phases of the self-tuning optimal excitation controller.

law corresponds to the adaptive immunity i.e. stage 2. Stages 1 and 2 constitute the design of the STOEC. The innate and adaptive immunity work simultaneously to eliminate any disturbance or oscillation introduced in the system. This corresponds to the operation stage in the flowchart. For stage 2 and operation stage, only the B cell mediated humoral immune response is considered.

The following subsections describe various steps involved in the optimal design of the excitation control system; OEC (stage 1), the immune system based self-tuning control system, STOEC (stage 2), and the operation stage of the STOEC respectively.

A. Design Phase

This phase consists of two stages, as mentioned above, Stage 1 for the optimal and Stage 2 for the self-tuning of the excitation control system design respectively.

1) Stage 1 (Optimal Excitation Controller Using Modified CSA):

The optimal parameters of the excitation controller are determined using modified CSA. The cost function for the optimization is the integrated transient response area of the voltage deviations of the generator during disturbances. The cost function takes into consideration the minimization of the overshoot and the settling time of the deviation in voltage. The CSA aims to minimize the cost function given by (8).

$$J = J_{PL\ 1} + J_{PL\ 2} \tag{8}$$

In this study, the optimization is carried out by subjecting the shipboard power system first to a pulsed load of 750 ms followed by a pulsed load of 500 ms as shown in Fig. 5.
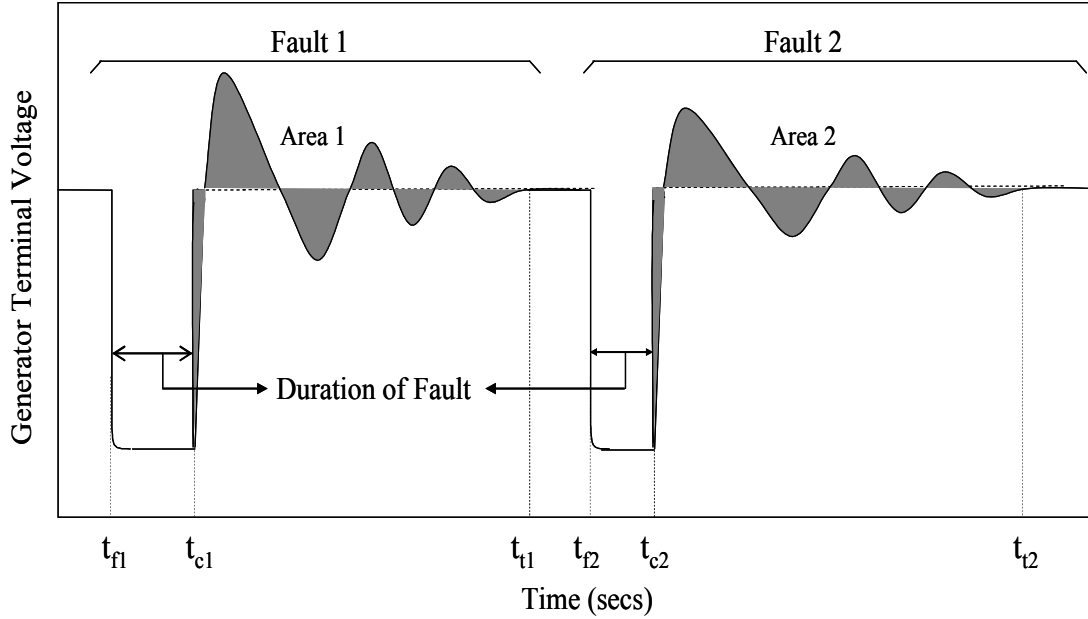
Fig. 5. Transient area under the curve is the cost function minimized for optimization.

The transient area under the generator terminal voltage response for the first pulsed load is given by

$$J_{PL1} = \sum_{t = t_{c1}}^{t_{t1} / \Delta t} (\Delta V_T (t)) \times (A \times (t - t_{c1}) \times \Delta t) \tag{9}$$

where $\Delta V_T(t)$ is the voltage deviation i.e. deviation of generator terminal voltage from the steady state reference value, A is weighting factor, t_{c1} and t_{t1} are the start and end time instants, respectively, considered for the transient area calculation, t_{c1} is also the time at which the fault is cleared, Δt is the terminal voltage signal sampling period and t is the simulation time in seconds.

Similarly, the transient area under the generator terminal voltage response for the second pulsed load is given by

$$J_{PL2} = \sum_{t=t_{c2}}^{t_{t2}/\Delta t} (\Delta V_T (t)) \times (A \times (t - t_{c2}) \times \Delta t) \tag{10}$$

where t_{c2} and t_{t2} are the start and end time instants respectively, considered for the transient area calculation, and t_{c2} is also the time at which the fault is cleared.

2) Stage 2 (Immune Based Self-Tuning Controller Using Immune Feedback Law):

This stage describes how the optimal parameters of the excitation system designed in Stage 1 are self-tuned dynamically during pulsed loads to maximize damping. The design here is analogous to the humoral B-cell mediated adaptive immune response of the human body. The optimal parameters of the excitation controller obtained above are made adaptive (only during transients) using the immune feedback law. The amount of foreign materials (antigens) at k^{th} generation can be defined as *Ag(k)*, which in this study is the deviation in the generator terminal voltage ΔV_T. The output from the helper T cells stimulated by the antigen is given by

$$T_H(k) = m \Delta V_T(k) \tag{11}$$

where *m* is the stimulation factor whose sign is positive. The response of the helper T cells is directly proportional to the antigens present in the system. Suppressor T cells inhibit other cell activities and their effect on B cells is given by

$$T_S(k) = m' f\left(\frac{\Delta V_T(k)}{\Delta V_T(k-1)}\right) \Delta V_T(k) \tag{12}$$

where *m'* is the positive suppression factor and *f(x)* is a nonlinear function introduced to take into account the effect of the reaction between the antibody (changes in controller

parameter behavior) and the antigen (controller input/disturbance). The response of the helper T cells is suppressed when the output of function *f(x)* is large i.e. suppression is directly proportional to the function *f(x)*. *f(x)* is large only when the ratio of the antigen at *(k)* is less as compared to the antigen at *(k-1)*. The function *f(x)* is defined as

$$f(x) = \exp\left(-x^2\right) \tag{13}$$

where the output of the function is limited within the interval [0, 1]. The square is introduced in *f(x)* to consider only the magnitude of the deviations in terminal voltage. This function is used as it can help to effectively suppress the action of the helper cells if the number of antigens is very less. Conversely, if the number of antigens is increased the exponential function would be a very small value and the suppressor cells will not be activated.

The total stimulation received by B cells, *B(k)*, is given by (14) and is known as the immune feedback law. It is the difference of the stimulation it receives from the helper T cells and the inhibition from the suppressor T cells. The changes in the controller parameters, *B(k)*, are responsible for fast damping of the deviations in the terminal voltage.

$$B(k) = T_H(k) - T_S(k) = g(k)\,\Delta V_T\ (k) \tag{14}$$

where

$$g(k) = m - m'f\left(\frac{\Delta V_T(k)}{\Delta V_T(k-1)}\right) \tag{15}$$

The mechanism of adaptation of parameters for the excitation controller based on the immune feedback law is depicted in Fig. 6. The excitation controller has three

parameters (K, T_1, and T_2); therefore three sets of equations, (16) to (18), are required to dynamically change these parameters.

$$\Delta K(k) = T_{H1}(k) - T_{S1}(k)$$

$$\Delta K(k) = \left[m_1 - m_2 f\left(\frac{\Delta V_T(k)}{\Delta V_T(k-1)} \right) \right] \Delta V_T(k) \tag{16}$$

$$\Delta T_1(k) = T_{H2}(k) - T_{S2}(k)$$

$$\Delta T_1(k) = \left[m_3 - m_4 f\left(\frac{\Delta V_T(k)}{\Delta V_T(k-1)} \right) \right] \Delta V_T(k) \tag{17}$$

$$\Delta T_2(k) = T_{H3}(k) - T_{S3}(k)$$

$$\Delta T_2(k) = \left[m_5 - m_6 f\left(\frac{\Delta V_T(k)}{\Delta V_T(k-1)} \right) \right] \Delta V_T(k) \tag{18}$$

The stimulation factors $m = [m_1, m_3,$ and $m_5]$ control speed of response, and suppression factors $m' = [m_2, m_4,$ and $m_6]$ and function $f(x)$ control the stabilization effect i.e. settling time. The performance of the immune feedback law greatly depends on how these factors are selected. Therefore, the CSA is used to determine the optimal values of the stimulation and suppression factors, $m = [m_1, m_3,$ and $m_5]$ and $m' = [m_2, m_4,$ and $m_6]$. The cost function minimized by CSA is again the integrated transient response area of the voltage deviations of the generator during disturbances. But for this optimization, three pulsed loads (250 ms, 750 ms and 1 s applied at 5 s, 10 s and 15 s respectively) are applied to calculate the cost function as given in (19). This is done to obtain optimal values of parameters m_1 to m_6 for different types of pulsed loads in the system.

$$J' = J'_{PL\,1} + J'_{PL\,2} + J'_{PL\,3} \qquad (19)$$

where J'_{PL1}, J'_{PL2} and J'_{PL3} are the transient response areas of voltage deviation for the

three pulsed loads.
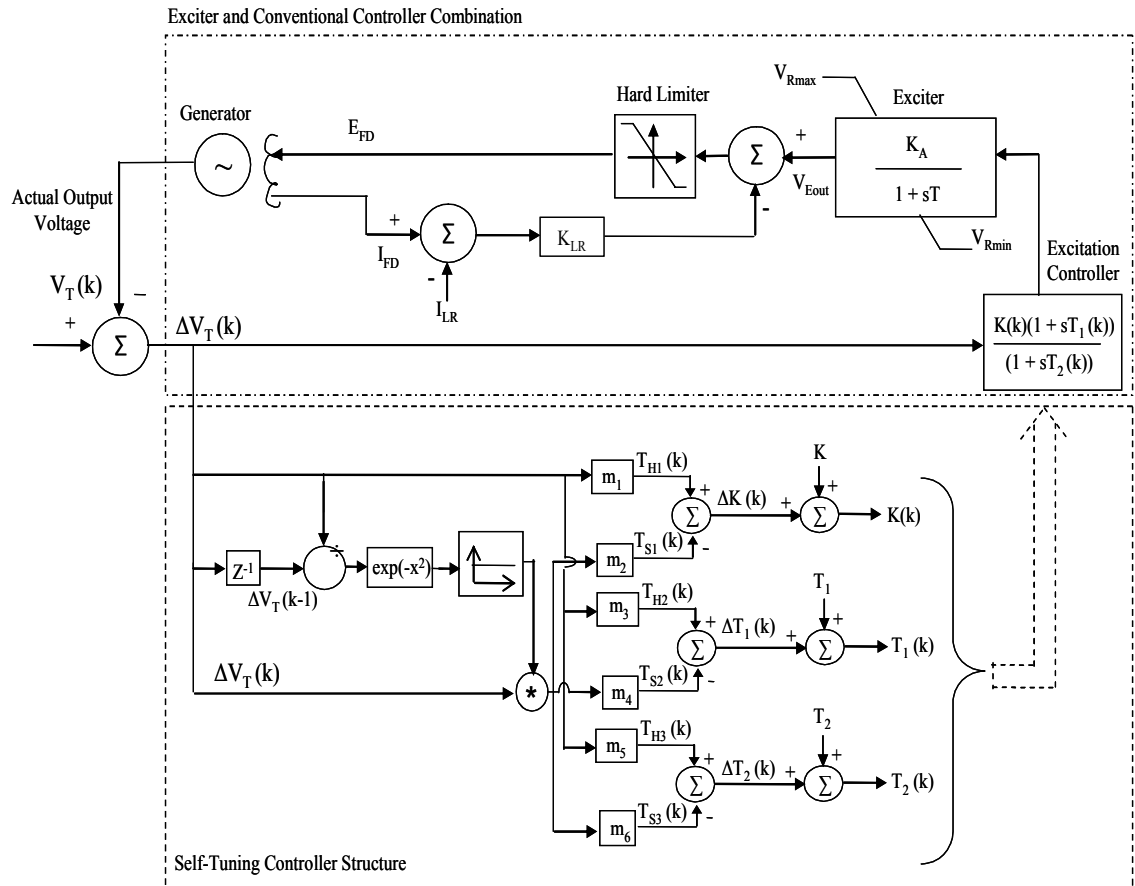

Fig. 6. Self-tuning optimal excitation controller.

B. Operation Phase (Self-Tuning Optimal Excitation Controller)

The operation phase corresponds to the self-tuning optimal excitation control. The

immune feedback law is implemented using the three equations given in (16) to (18).

Using the optimal values of the stimulation and suppression factors (m_1 to m_6) the optimal

parameters of the excitation controller (K, T_1 and T_2) are self-tuned during transients by applying the immune feedback law according to (20) to (22)

$$K(k) = K + \Delta K(k) \tag{20}$$

$$T_1(k) = T_1 + \Delta T_1(k) \tag{21}$$

$$T_2(k) = T_2 + \Delta T_2(k) \tag{22}$$

The immune feedback law, changes the values of the optimal parameters dynamically with deviation in the generator terminal voltage. Thus, the excitation controller parameters are self tuned during pulsed load conditions to minimize the oscillations in the system and improve the damping performance.

VI. EXCITATION CONTROLLER SIMULATION RESULTS

The electric ship power system given in Fig. 3 is simulated using the power system simulation software PSCAD/ EMTDC [32]. The AIS and the CSA are implemented in FORTRAN. The modified CSA used for the optimizations has a population of 20 antibodies; 5 antibodies with the highest affinity are selected for cloning and 4 clones each are generated for the 5 antibodies. Thus, for determining the optimal controller parameters and the optimal values of stimulation and suppression factors $N = 20$, $C = 5$, $\beta = 0.2$, $N_C = 4$.

Simulation results are presented to compare the performance of OEC with the non optimal controller and further comparison of the performance of the OEC controller with

that of the STOEC is presented. The following subsections present the responses of the OEC and the STOEC for different pulsed loads, respectively.

A. Optimal Excitation Controller

The response of the controller with parameters optimized by the CSA is compared with the response of a controller whose parameters are manually tuned [33] to give satisfactory performance. The manually tuned parameters obtained for best time response for the excitation controller are as follows: $K = 250$, $T_1 = 0.2$, $T_2 = 0.05$. The cost function minimized is the integrated transient response area of the voltage deviations of the generator when pulsed loads of 500 ms and 750 ms are applied to the shipboard power system and is given in (8). The CSA optimization to determine the generator parameters is carried over 10 trials.

The average fitness (over the 10 trials) during successive iterations of the algorithm is shown in Fig. 7. This fitness corresponds to the average fitness of the antibody with the highest affinity i.e. average of Ab_{best} of each trial. The optimal values obtained for the 10 trials and their corresponding fitness are given in Table B.2 in the Appendix. The best optimal values obtained (using modified CSA) for the generator excitation controller are:

$$K = 241.3083, T_1 = 0.5273, \text{ and } T_2 = 0.0021.$$

The limits used for optimization of these parameters are:

$$10 < K < 500 \qquad 0.001 < T_1 < 0.75 \qquad 0.001 < T_2 < 0.75.$$

The mean fitness and the standard deviation after 40 iterations is 3.5003±0.8259.
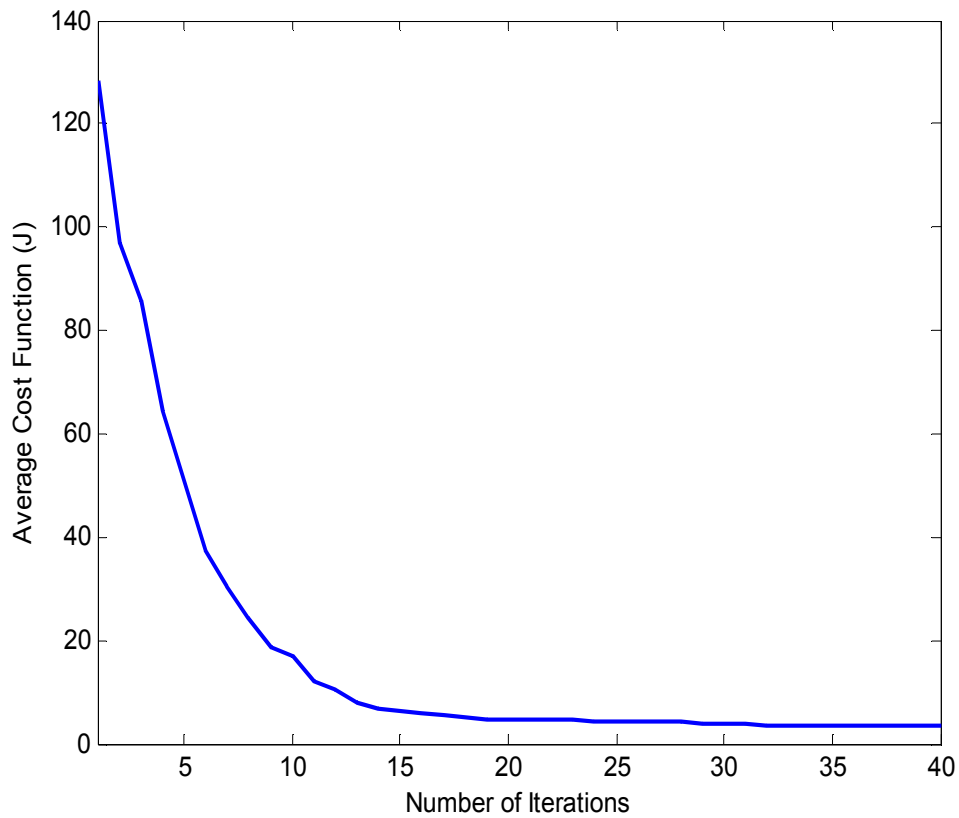
Fig. 7. Fitness over successive iterations for design of the optimal controller.

The response of the excitation controller with modified CSA determined optimal parameters (OEC) has been compared with that of an excitation controller with manually tuned parameters (non-optimal excitation controller referred as NOEC) below. The comparison is made for a pulsed load of duration 750 ms. The plots for the generator terminal voltage and generator reactive power, and the field voltage and field current are shown in Figs. 8 and 9, respectively.

It is seen that the performance of the OEC is better than that of the NOEC and it efficiently restores the system to its steady state.
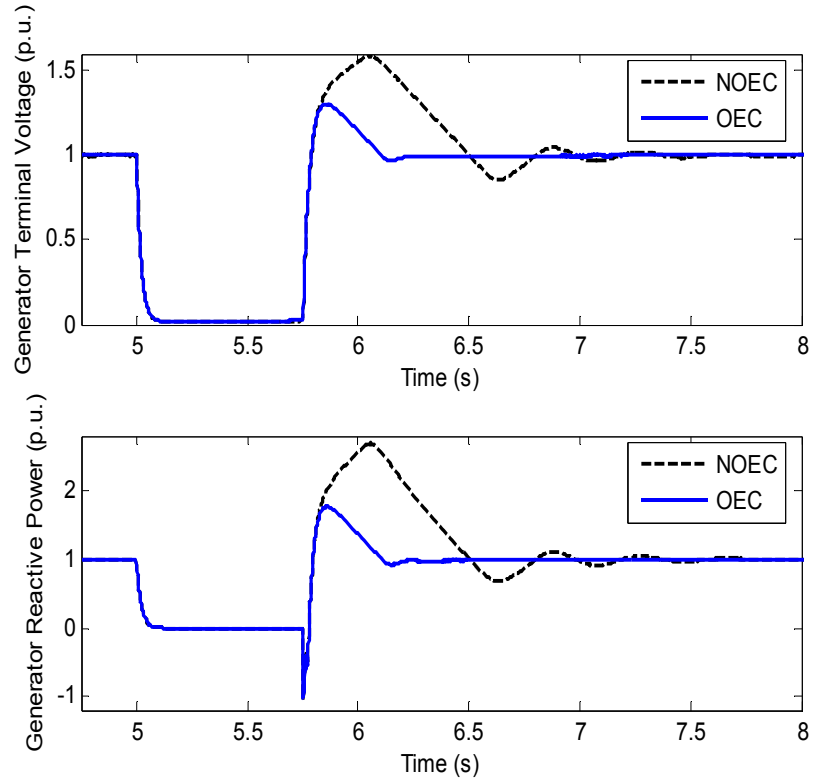
Fig. 8. Generator terminal voltage and reactive power for pulsed load of duration 750 ms.
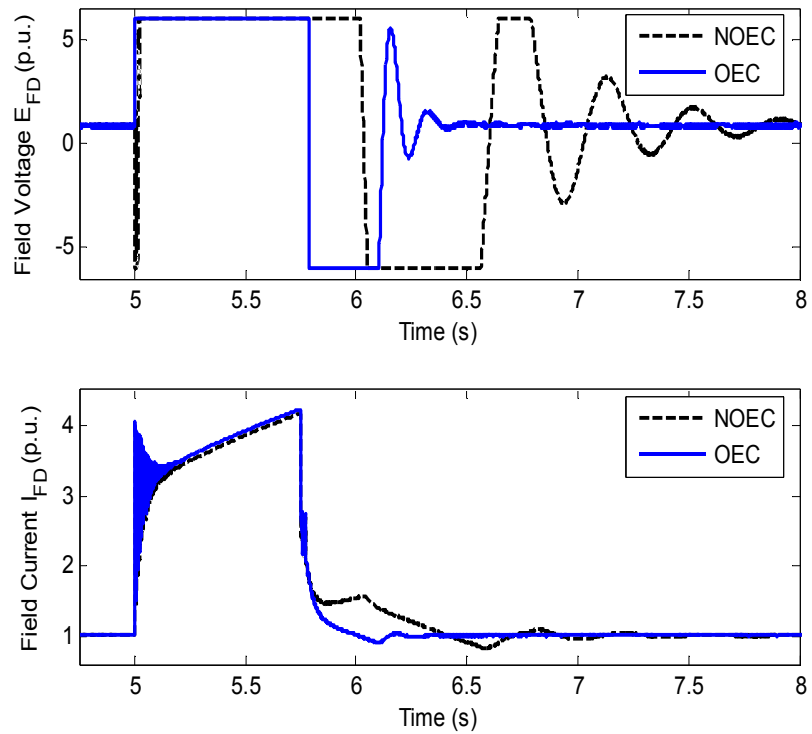
Fig. 9. Field voltage and field current for pulsed load of duration 750 ms.

It can clearly be seen that the controller with the CSA optimized parameters shows a better response in terms of damping the oscillations introduced in the system. The generator terminal voltage shows less deviations and the overshoot is significantly minimized. The generator reactive power also shows similar results. The settling time of the field voltage is minimized and consequently the reactive power of the generator attains it steady state value quickly. The field current of the excitation controller settles to its steady state value faster with OEC as compared to NOEC. Hence, the controller with modified CSA optimized parameters has better performance and lesser settling time, than a manually tuned controller.

B. Self-Tuning Optimal Excitation Controller

The adaptation of parameters of an optimal excitation controller using the immune feedback law improves the performance of the optimal controller. The immune feedback concept takes into consideration the deviation in the generator terminal voltage from the steady state value and adapts the excitation controller parameters accordingly. The cost function minimized by modified CSA for determining the optimal values of m_1 to m_6 is the integrated transient response area of the voltage deviations of the generator when three pulsed loads of 250 ms, 750 ms, and 1 s are applied sequentially. This cost function is given in (19). The optimal stimulation and suppression factors (m_1 to m_6) are determined using CSA for optimal excitation controller parameters (K, T_1, and T_2). Again, this is done over 10 trials. The optimal values of the stimulation and suppression factors obtained for the 10 trials and their corresponding fitness are given in Table B.3 in the Appendix. The average fitness (over 10 trials) during successive iterations of the

algorithm is shown in Fig. 10. The average fitness corresponds to the average fitness of the antibody with the highest affinity i.e. Ab_{best} for every iteration. The mean fitness and the standard deviation over 40 iterations is 1.6415 ± 0.9598. The following are the best set of optimal values obtained (using modified CSA) for the stimulation and suppression parameters m_1 to m_6 :

$m_1 = 0.0378$, $m_2 = 701.3316$, $m_3 = 0.4061$, $m_4 = 0.2976$, $m_5 = 0.0007$, $m_6 = 0.0007$.
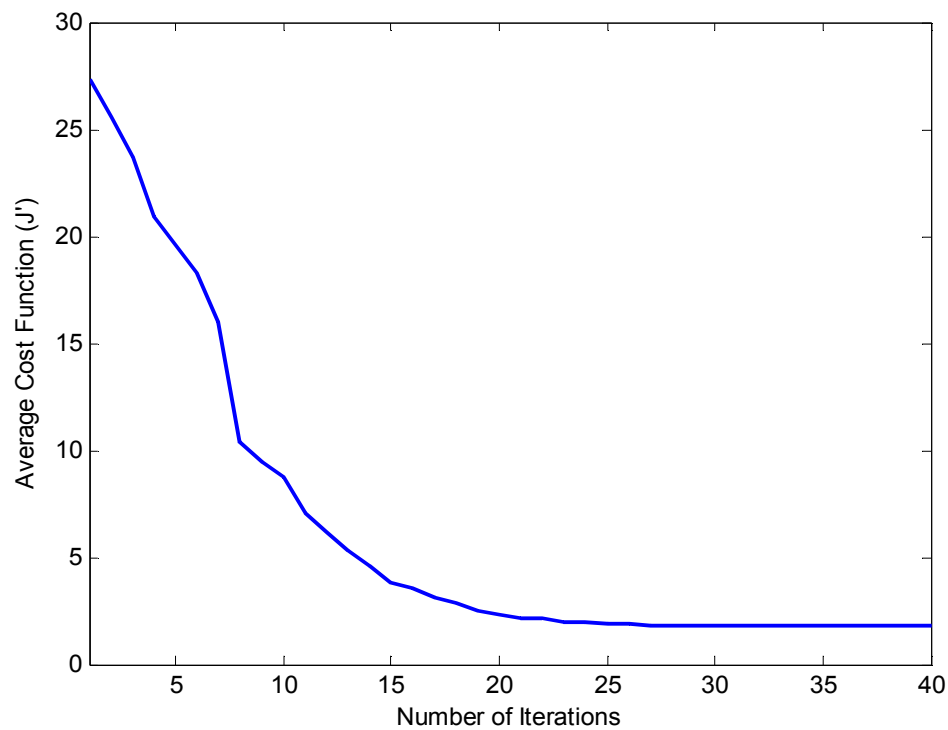
Fig. 10. Fitness over successive iterations for design of the self-tuning optimal controller.

The response of the OEC is now compared with that of the immune system based STOEC for pulsed loads of 500 ms and 1 s. The generator terminal voltage, generator reactive power, field voltage and field current for the two pulsed loads are shown in Figs. 11 to 14, respectively. The immune feedback law concept is applied using (16)-(18) and the parameters of the controller are updated using (20)-(22).
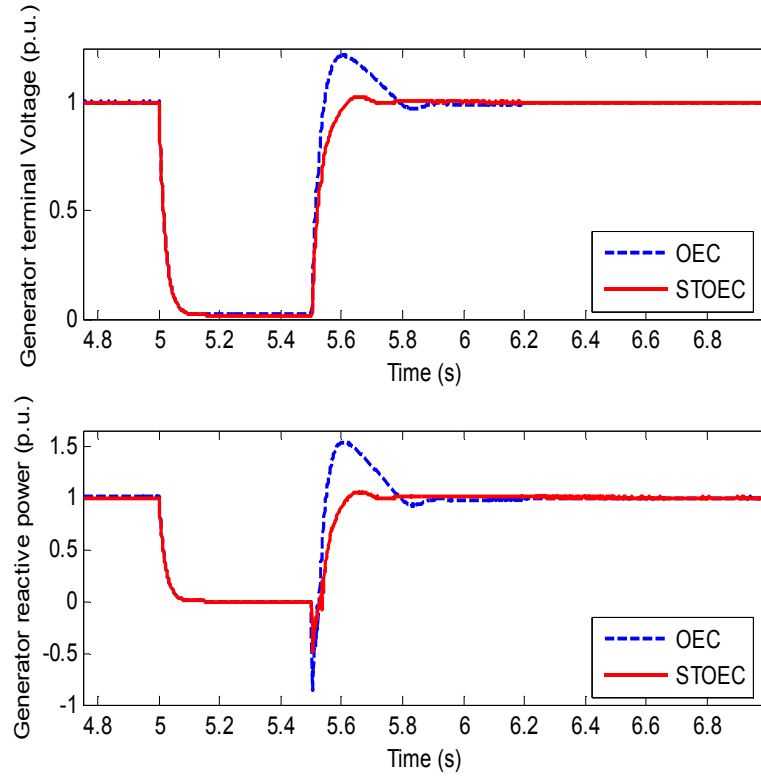
Fig. 11. Generator terminal voltage and reactive power for pulsed load of duration 500 ms.
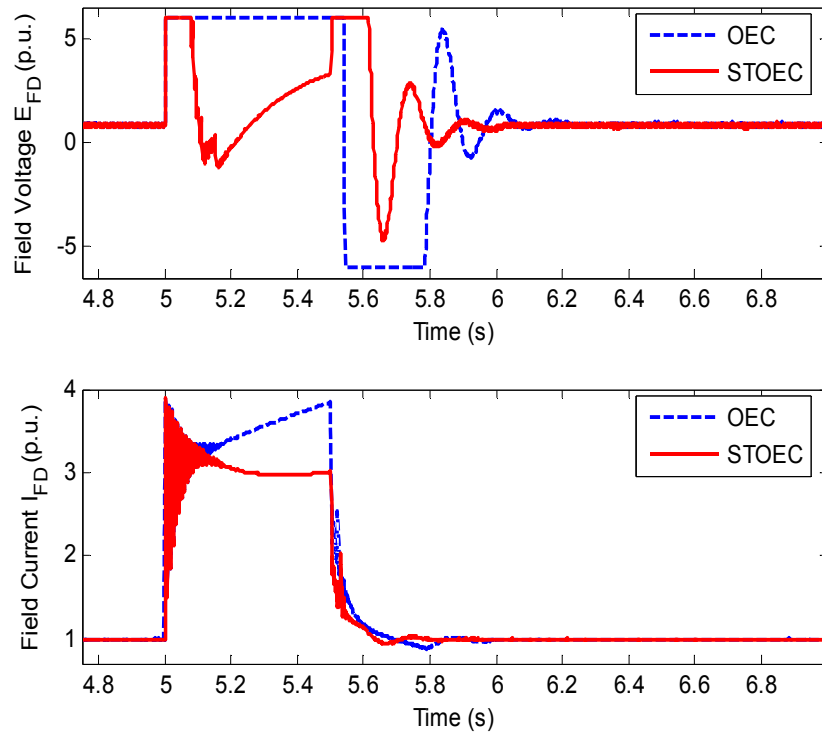
Fig. 12. Field voltage and field current for pulsed load of duration 500 ms.
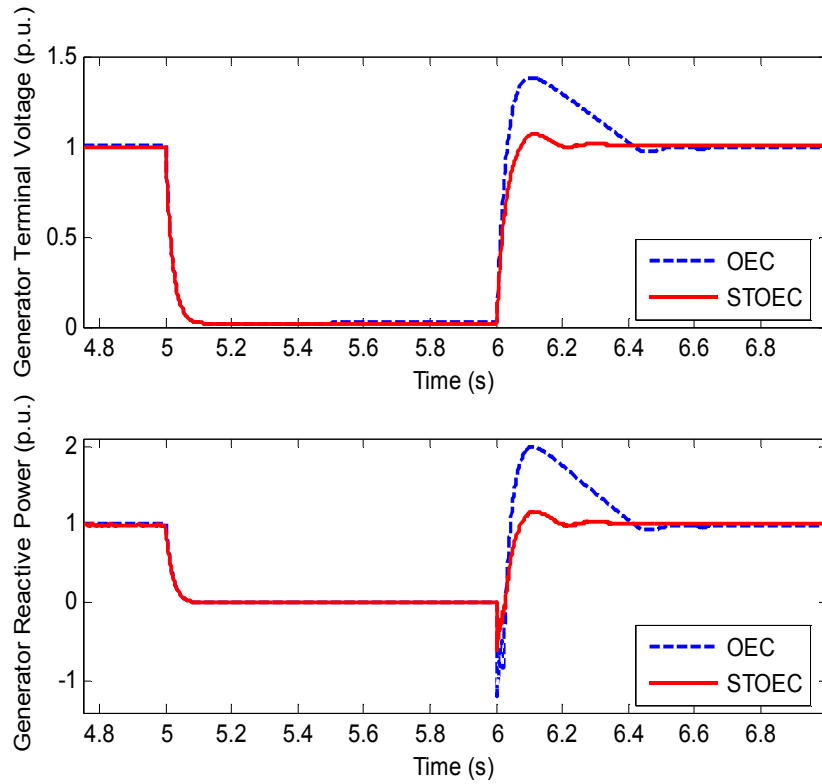
Fig. 13. Generator terminal voltage and reactive power for pulsed load of duration 1 s.
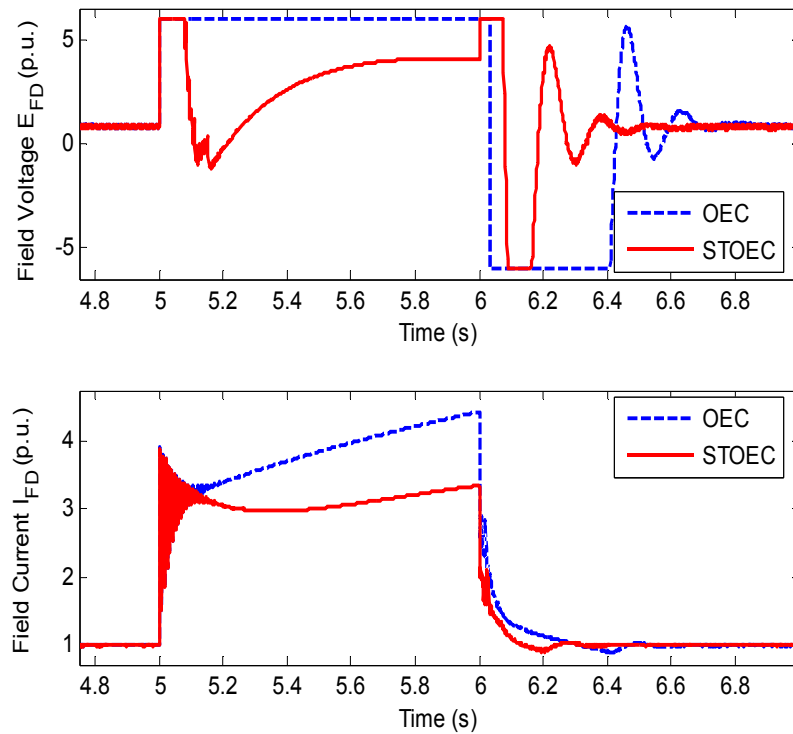
Fig. 14. Field voltage and field current for pulsed load of duration 1 s.

In Figs. 11 and 13 it is seen that the oscillations in the generator terminal voltage and reactive power are significantly minimized for the STOEC in comparison to the OEC. The overshoot for the STOEC is considerably reduced and the steady state value is attained quickly after the pulsed load is removed. Figs. 12 and 14 show that the field voltage settles down faster for the STOEC as compared to the OEC. During pulsed loads, the field current rises to high values for the OEC. But for STOEC, the increase in field current during a pulsed load is reduced. Thus, the I^2R loss during pulsed load is lower with a STOEC. This in turn enhances the life of the field circuit.

Fig. 15 depicts the variations in the excitation controller parameters K, T_1 and T_2, for a pulsed load of duration 1 s. The excitation controller parameters of the STOEC vary with terminal voltage deviations unlike the parameters of the OEC, which remain constant.
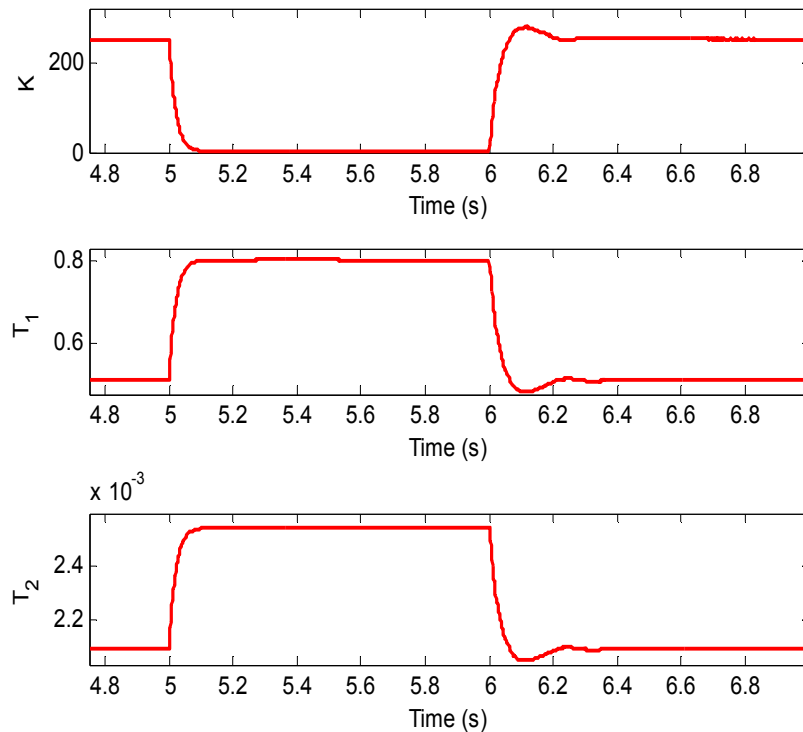
Fig. 15. Variation of K, T_1 and T_2 for pulsed load of duration 1 s.

From Figs. 11 to 14, it can be seen that the overall response of the STOEC is better than that of the OEC. This is because the excitation controller parameters vary with the deviations in generator terminal voltage as can be seen in Fig. 15. The gain of the controller almost drops to zero during the pulsed load. This in turn reduces the output of the controller fed to the exciter and constraints the field voltage. The time constants T_1 and T_2 also vary during pulsed loads to improve the damping performance and restore the system to its steady state. The time constants T_1 and T_2 increase during pulsed loads, this provides an additional phase lead during transients.

Adaptation of the controller parameters has resulted in an improved response and efficient damping during pulsed load conditions. Table V compares the maximum overshoot and the settling time (required for the generator terminal voltage to settle within ±2% of its steady state value) of OEC and STOEC for various pulsed loads. The settling time is calculated after the pulsed load is removed. Table VI gives the energy loss in the field circuit for various pulsed loads. The energy loss is calculated during the transients, until the field current first reaches the steady state value. The energy loss is given by

$$E_L = \sum_{t=t_{s1}}^{t_{s2}} \frac{1}{2}(I_{t-1}^2 + I_t^2)R_f \times \Delta t \tag{23}$$

where I_t and I_{t-1} are the field currents at any time t and t-1, respectively, R_f is the resistance in the field circuit, t_{s1} and t_{s2} are the time instances when the field current deviates from the steady state value and thereafter when it first returns to the steady state value, respectively, as shown in Fig. 16. Δt is the field current signal sampling period.
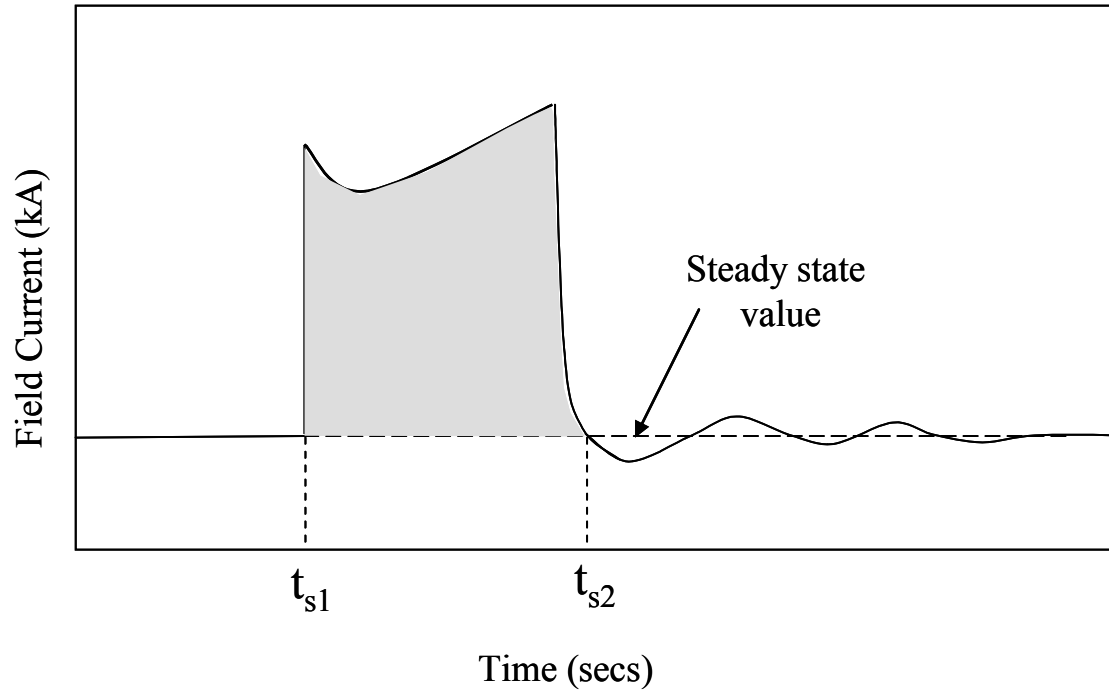
Fig. 16. Energy loss calculation during transients.

Table V

Maximum Overshoot and Settling Time for Different Pulsed Loads

Pulsed Load	Maximum Overshoot (%)			Settling Time (s)		
Duration (s)	OEC	STOEC	Improvement (%)	OEC	STOEC	Improvement (%)
0.10	6.8	6.3	7.35	0.23	0.17	26.09
0.20	10.7	4.4	58.87	0.28	0.08	71.42
0.30	14.3	3.6	74.82	0.31	0.16	48.38
0.40	17.8	3.6	79.77	0.34	0.16	52.94
0.50	21.5	4.0	81.39	0.37	0.16	56.76
0.60	25.1	5.1	79.68	0.39	0.16	58.97
0.70	28.6	6.2	78.32	0.42	0.17	59.52
0.80	37.9	7.7	79.68	0.45	0.18	60.00
0.90	35.0	9.2	73.71	0.47	0.19	59.57
1.0	37.8	10.3	72.75	0.49	0.20	59.18

Table VI

Energy Loss in Field Circuit for Different Pulsed Loads

Pulsed Load Duration (s)	Energy Loss		
	OEC (kJ)	STOEC (kJ)	Reduction (%)
0.10	3.6245	3.5939	0.85
0.20	7.1585	6.5916	7.92
0.30	11.0526	9.3955	14.99
0.40	15.3245	12.7091	17.07
0.50	19.9711	14.8329	25.73
0.60	25.0032	17.6851	29.27
0.70	30.3923	20.6787	31.96
0.80	36.0319	23.7921	33.97
0.90	42.0826	27.1124	35.57
1.0	48.3769	30.5475	36.86

It can be seen from Table V that the maximum overshoot is minimized considerably for the STOEC as compared to the OEC. As the duration of the pulsed load is increased, this drop in the overshoot becomes more significant. This is because the innate immunity of the system i.e. the OEC mostly handles pulsed loads of small duration. For pulsed loads of longer duration, the adaptive immunity kicks in i.e. STOEC and restores the system to its steady state much faster. The settling time is also greatly reduced for the STOEC as compared to the OEC.

Table VI shows that the STOEC can reduce the energy loss in the field circuit up to 36.86% i.e. 17.8294 kJ. Hence, the STOEC greatly minimizes the maximum overshoot and the settling time of the generator terminal voltage, and reduces the energy loss in the field circuit.

VII. CONCLUSION

AIS based algorithms for optimization and control have been presented in this paper. Modified CSA has been used for optimization of four benchmark functions and it is seen that modified CSA has the ability to produce better solutions and converges quickly as compared to PSO and GA for different dimensions and population sizes. Modified CSA is then used for design of an OEC which shows better response in terms of damping the oscillations introduced in the system as compared to the non optimal controller. It minimizes the overshoot and settling time of oscillations in the generator terminal voltage and reactive power. The performance of the OEC is further improved by application of the immune feedback law. The design of the STOEC is achieved by incorporation of the self-tuning characteristics inspired by the humoral adaptive immune response of the human body. The OEC provides innate immunity from system oscillations while the adaptation of optimal parameters provides the adaptive immunity. The STOEC reduces the overshoot and settling time significantly. The power (I^2R) losses are considerably reduced (up to 36.86%) when using STOEC as the field current does not attain high values even during pulsed load conditions. This in turn enhances the life of the field circuit. STOEC adapts to the deviations in the terminal voltage and minimizes the oscillations in the system. Pulsed loads on an electric ship require efficient damping and robust functioning to maintain power continuity. This is successfully achieved using the STOEC.

Future work involves real time implementation of the STOEC on the real-time digital simulator. The STOEC proposed does not include the memory cells to remember the response to a particular antigen. Future work will also involve the inclusion of

memory cells to store the response to a particular type of antigen for future use when similar antigens are encountered. This would result in the improvement of controller's speed of response for previously seen pulsed loads.

VIII. REFERENCES

[1] L. N. de Castro, F. J. V. Zuben, "aiNet: An Artificial Immune Network for Data Analysis" in *Data Mining: A Heuristic Approach.* Idea Group Publishing, USA, March, 2001, pp.231-259.

[2] S. Forrest, A. S. Perelson, L. Allen, R. Cherukuri, "Self-Nonself Discrimination in a Computer," *IEEE Proceedings of Computer Society Symposium on Research in Security and Privacy,* May 16-18, 1994, pp. 202-212.

[3] Y. Luo, C. Wang, X. Tu, "Application of Artificial Immune Algorithm to Multimodal Function Optimization," *WCICA World Congress on Intelligent Control and Automation*, June 2004, vol. 3, pp. 2248-2252.

[4] N. K. Jerne, *Towards a Network Theory of the Immune System,* Ann Immunol. (Paris), 125C (1-2), Jan 1974, pp. 373-389.

[5] S. Huang, "Application of Immune-based Optimization method for Fault-section Estimation in a Distribution System," *IEEE Transactions on Power Delivery*, July 2002, vol. 17, issue 3, pp. 779-784.

[6] D. Lee, K. Sim, "Artificial Immune Network Based Cooperative Control in Collective Autonomous Mobile Robots," *IEEE International Workshop on Robot and Human Communication,* Sept. 1997, pp. 58-63.

[7] B. Wang, S. Wang, J. Zhuang, "A Distributed Immune Algorithm for Learning Experience in Complex Industrial Processes Control," *International Conference on Machine Learning and Cybernetics*, Nov. 2003, vol.4, pp. 2138-2141.

[8] T. Lin, H. Su, Y. Peng, Z. Lei, "Research on the Network Intrusion Detection Based on the Immune System," *International Conference on Machine Learning and Cybernetics*, Aug. 2006, pp. 4479-4482.

[9]   D. Das, N. S. Majumdar, "Anomaly Detection in Multidimensional Data Using Negative Selection Algorithm," *Proceeding of Congresson Evolutionary Computation*, May 2002, vol. 2, pp. 1039-1044.

[10]   J. Yu, H. Zhou, "Fault Diagnosis Model of Transformer Based on Immune Algorithm," *IEEE PES Transmission and Distribution Conference,* 2005, pp. 1-4.

[11]   G. C. Liao, "Application of an Immune Algorithm to the Short-term Unit Commitment Problem in Power System Operation," *IEEE Proceedings of Generation, Transmission and Distribution*, May 2006, vol. 153, issue 3, pp. 309-320.

[12]   P. K. Harmer, P. D. Williams, G. H. Gunsch, G. B. Lamont, "An Artificial Immune System Architecture for Computer Security Applications," *IEEE Transactions on Evolutionary Computation*, June 2002, vol. 6, issue 3, pp. 252-280.

[13]   D. Dasgupta, Y. Cao, C. Yang, "An Immunogenetic Approach to Spectra Recognition," *Proceedings of International Conference on Genetic and Evolution Computation*, July 1999, pp. 149-155.

[14]   L. Fang, L. Chaoyang, "A Multiview Face Recognition Based on Combined Feature with Clonal Selection," *International Conference on Signal processing,* Aug 2004, vol. 2, pp. 1380-1384.

[15]   F. Campelo, F. G. Guimaraes, H. Igarashi, J. A. Ramirez, "A Clonal Selection Algorithm for Optimization in Electromagnetics," *IEEE Transactions on Magnetics*, May 2005, vol. 41, issue 5, pp. 1736-1739.

[16]   L. Wang, B. Hirsbrunner, "An Evolutionary Algorithm with Population Immunity and its Application on Autonomous Robot Control," *Congress on Evolutionary Computation*, Dec. 2003, vol. 1, pp. 397-404.

[17]   R. E. Hebner, "Electric ship power system – Research at the University of Texas, Austin," *IEEE Electric Ship Technologies Symposium*, July 2005, pp. 34-38.

[18]   V. Arcidiacono, S. Castellan, R. Menis, G. Sulligoi, "Integrated Voltage and Reactive Power Control for All Electric Ship Power Systems," *IEEE International Symposium on Power Electronics, Electric Drives, Automation and Motion,* May 23-26, 2006, pp. 878-882.

[19]   Z. W. Vilar, R. A. Dougal, "Effectiveness of Generator Control Strategies on Meeting Pulsed Load Requirements in Ship Electric Systems," *IEEE Electric Ship Technologies Symposium*, July 25-27,   2005, pp. 459-462.

[20]   E. L. Zivi, "Integrated Shipboard Power and Automation Control Challenge Problem," *IEEE Power Engineering Society Summer Meeting,* vol. 1, 2002, pp. 325-330.

[21] D. Dasgupta, "Advances in Artificial Immune systems," *IEEE Computational Intelligence Magazine,* vol. 1, no. 4, Nov., 2006, pp. 40-49.

[22] N. K. Jerne, *Towards a Network Theory of the Immune System,* Ann Immunol. (Paris), 125C (1-2), Jan 1974, pp. 373-389.

[23] L. N. de Castro, F. J. V. Zuben, "aiNet: An Artificial Immune Network for Data Analysis," in *Data Mining: A Heuristic Approach.* Idea Group Publishing, USA, March, 2001, pp.231-259.

[24] S. Forrest, A. S. Perelson, L. Allen, R. Cherukuri, "Self-Nonself Discrimination in a Computer," *IEEE Proceedings of Computer Society Symposium on Research in Security and Privacy,* May 16-18, 1994, pp. 202-212.

[25] C. A. Janeway, P. Travers, M. Walport, M. J. Shlomchik, *Immunobiology*, Garland Science, 6th edition, 2005, ISBN 0-8153-4101-6.

[26] F. M. Burnet, "Clonal Selection and After", *Theoretical Immunology,* In Bell G I, A S Perelson, G H Pimbley eds, New York, Marcel DekkerInc., 1978, pp. 63-85.

[27] L. N. de Castro, F. J. Von Zuben, "Learning and Optimization Using the Clonal Selection Principle," *IEEE Transactions on Evolutionary Computations,* June 2002, vol. 6, no. 3, pp. 239-251.

[28] Y. Shi, R. C. Eberhart, "Empirical Study of Particle Swarm Optimization," *Congress on Evolutionary Computation*, July 1999, vol. 3, pp. 1945-1950.

[29] Z. Jin, G. Liu, W. Wen, "Clonal Selection Algorithm with Hyper Mutation and Spatial Clone Extension," *International Conference on Computational Intelligence and Security*, Nov. 2006, vol. 1, pp. 402-405.

[30] B. Cassimere, R. Valdez, S. Sudhoff , S. Pekarck, B. Kuhn, D. Delisle, E. L. Zivi, "System Impact of Pulsed Power Loads on a Laboratory Scale Integrated Fight Through Power (IFTP)," *IEEE Electric Ship Technologies Symposium,* July 25-27, 2005, pp.176-183.

[31] IEEE Std. 421.5-1992 IEEE Recommended Practice for Excitation System Models for Power System Stability Studies - Description.

[32] S. S. Kalsi, O. Nayak, "Ship Electrical System Simulation," *Electric Ship Technologies Symposium,*25-27 July, 2005, pp. 63-69.

[33] K. Ogata, *Modern Control Engineering,* Prentice Hall; 3rd Edition, 1996, ISBN 0-1322-7307-1.

APPENDIX A.

APPENDIX FOR PAPER 1

Table A.1

Two Area Power System PSS Parameters

Generator	Kundur's parameters	PSO optimized parameters	CSA optimized parameters
G1-G4	$K = 20.0$, $T_1 = 0.05$, $T_2 = 0.02$, $T_3 = 3.0$ $T_4 = 5.4$	$K = 22.397$, $T_1 = 0.059$, $T_2 = 0.01$, $T_3 = 4.7478$, $T_4 = 4.4670$	$K = 23.869$, $T_1 = 0.0626$, $T_2 = 0.01$, $T_3 = 6.6565$, $T_4 = 6.4803$

APPENDIX B.

APPENDIX FOR PAPER 2

Table B.1

Values of Parameters in the Conventional Linear Excitation Controller (Fig. 3.)

Conventional Linear Excitation Controller Parameter	Value(p.u.)
Exciter output current limit reference, I_{LR}	4.4
Exciter output current limiter gain, K_{LR}	4.54
Maximum regulator output limit, V_{Rmax}	999
Minimum regulator output limit, V_{Rmin}	-999
Maximum limit for the hard limiter	6.0
Minimum limit for the hard limiter	-6.0

Table B.2

Optimal Controller Parameters Obtained for 10 Trials

Trials	K	T_1	T_2	Fitness
1	**241.30833**	**0.52735**	**0.00212**	**2.16347**
2	249.53559	0.43690	0.03179	4.33944
3	253.49660	0.42877	0.02831	3.70731
4	255.42591	0.46684	0.01801	2.32979
5	261.58787	0.43458	0.00885	3.20305
6	239.28941	0.55623	0.00868	2.85759
7	261.01969	0.41763	0.02436	3.86520
8	262.25196	0.39393	0.02436	4.53025
9	261.82728	0.40877	0.02464	4.13254
10	261.20890	0.41547	0.02164	3.87461

Table B.3

Optimal Stimulation and Suppression Factors Obtained for 10 Trials

Trial	m_1	m_2	m_3	m_4	m_5	m_6	Fitness
1	**0.0378**	**701.3316**	**0.4061**	**0.2976**	**0.0007**	**0.0007**	**1.0088**
2	0.0296	687.542	0.5148	0.3442	0.0009	0.0008	2.6169
3	0.0548	679.782	0.6221	0.1545	0.0015	0.0019	3.6689
4	0.0292	685.145	0.5267	0.3981	0.0009	0.0008	2.6166
5	0.0371	702.4831	0.4120	0.2914	0.0007	0.0007	1.0088
6	0.0376	697.7330	0.5590	0.4098	0.0010	0.0010	1.1185
7	0.0377	699.1490	0.5602	0.4106	0.0010	0.0010	1.1366
8	0.0377	698.4382	0.5596	0.4102	0.0010	0.0010	1.1053
9	0.0493	693.8381	1.5772	0.8557	0.0027	0.0022	1.0295
10	0.0377	698.4922	0.5596	0.4102	0.0010	0.0010	1.1052

VITA

Mani Hunjan, was born on May 20, 1982 in Jhansi, India. She graduated in June 2004 from Punjab Technical University, India with Bachelor of Technology degree in Electrical Engineering. She received a Master of Science degree from University of Missouri, Rolla in August 2007 in Electrical Engineering. Her research focuses on artificial immune system and its application for optimization and control in power systems.